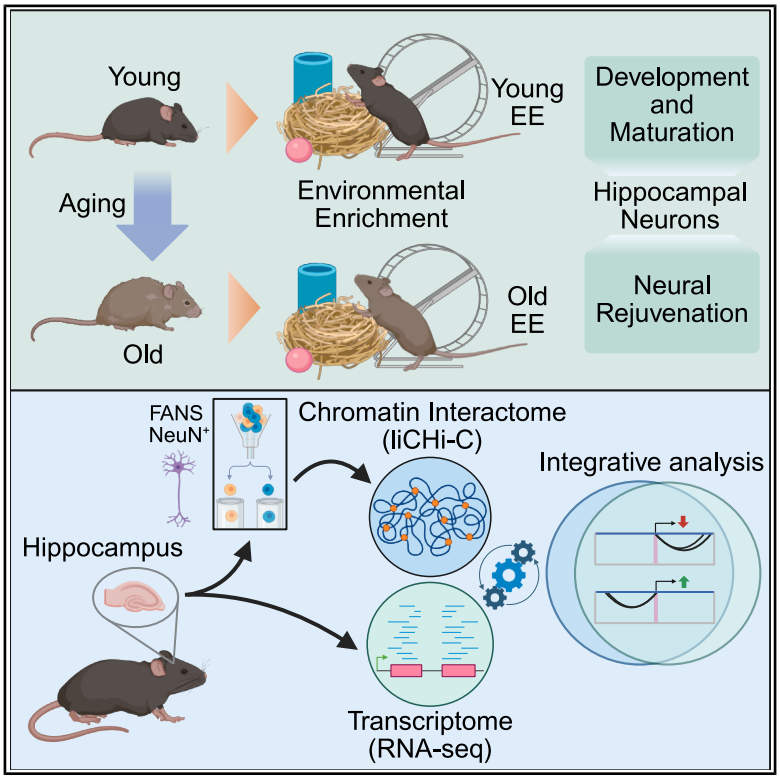
Cell Reports

Article

Age-dependent effect of environmental enrichment on the neural 3D chromatin interactome

Graphical abstract



Highlights

- We report the functional 3D chromatin interactomes in neurons of young and old mice
- Environmental enrichment (EE) induces age-dependent changes in neural interactions
- EE promotes aging-like changes in the 3D chromatin interactome of young mice
- In old mice, EE reverts several age-related changes in the neural interactome

Authors

Javier Gancedo-Verdejo, Rocío G. Urdinguio, Juan Ramón Tejedor, ..., Biola M. Javierre, Agustín F. Fernández, Mario F. Fraga

Correspondence

rgurdinguio@cinn.es (R.G.U.), agustin.fernandez@cinn.es (A.F.F.), mffraga@cinn.es (M.F.F.)

In brief

Gancedo-Verdejo et al. reveal age-associated molecular changes in mouse hippocampus and an age-dependent effect of environmental enrichment, focusing on 3D chromatin structure and gene expression. Environmental enrichment promotes aging-like changes in young mice, likely related to brain maturation; conversely, it reverts age-related alterations in old mice, suggesting neuronal rejuvenation.

Gancedo-Verdejo et al., 2025, Cell Reports *44*, 116182
September 23, 2025 © 2025 The Authors. Published by Elsevier Inc.
https://doi.org/10.1016/j.celrep.2025.116182

CellPress

Cell Reports

CellPress
OPEN ACCESS

Article

Age-dependent effect of environmental enrichment on the neural 3D chromatin interactome

Javier Gancedo-Verdejo,[1,2,3,4,13] Rocío G. Urdinguio,[1,2,3,4,13,*] Juan Ramón Tejedor,[1,2,3,4] Raúl F. Pérez,[1,2,3,5,6] Alfonso Peñarroya,[1,2,3] Pablo Santamarina-Ojeda,[1,2,3,4] Annalisa Roberti,[1,2,3,4] Jennifer M. Kefauver,[1,2,3,4] Carlota Álvarez-Díaz,[1,2,3] Mar Rodríguez-Santamaría,[2,3,7] José Luis Trejo,[8] Laureano Tomás-Daza,[9,10] Llorenç Rovirosa,[9] Biola M. Javierre,[9,11] Agustín F. Fernández,[1,2,3,4,*] and Mario F. Fraga[1,2,3,4,12,14,*]

[1]Cancer Epigenetics and Nanomedicine Laboratory, Nanomaterials and Nanotechnology Research Center (CINN), Spanish National Research Council (CSIC), 33940 El Entrego, Asturias, Spain
[2]Health Research Institute of the Principality of Asturias (ISPA), 33011 Oviedo, Asturias, Spain
[3]University Institute of Oncology of Asturias (IUOPA), University of Oviedo, 33006 Oviedo, Asturias, Spain
[4]Spanish Biomedical Research Network in Rare Diseases (CIBERER), 33011 Oviedo, Asturias, Spain
[5]Fundació de Recerca Clínic Barcelona – Institut d'Investigacions Biomèdiques August Pi i Sunyer (IDIBAPS), 08036 Barcelona, Cataluña, Spain
[6]Department of Biochemistry and Molecular Biology, Complutense University of Madrid, 28040 Madrid, Comunidad de Madrid, Spain
[7]Animal Unit and Preclinical Imaging, University of Oviedo, 33006 Oviedo, Asturias, Spain
[8]Department of Translational Neuroscience, Cajal Institute (IC), Spanish National Research Council (CSIC), 28002 Madrid, Comunidad de Madrid, Spain
[9]Josep Carreras Leukaemia Research Institute (IJC), 08916 Badalona, Cataluña, Spain
[10]Barcelona Supercomputing Center, 08034 Barcelona, Cataluña, Spain
[11]Institute for Health Science Research Germans Trias i Pujol (IGTP), 08916 Badalona, Cataluña, Spain
[12]Department of Organisms and Systems Biology, University of Oviedo, 33006 Oviedo, Asturias, Spain
[13]These authors contributed equally
[14]Lead contact
*Correspondence: rgurdinguio@cinn.es (R.G.U.), agustin.fernandez@cinn.es (A.F.F.), mffraga@cinn.es (M.F.F.)
https://doi.org/10.1016/j.celrep.2025.116182

SUMMARY

Aging is a multifactorial biological process resulting in physiological and cellular decline. However, our understanding of age-related changes in 3D genome organization and the effect of external interventions on this process remains limited. Here, we describe alterations in the landscape of the 3D chromatin interactome upon aging, utilizing the low-input promoter capture Hi-C (liCHi-C) technique with mouse hippocampal neurons. We also integrated liCHi-C data with RNA sequencing (RNA-seq) data to identify functional implications. Furthermore, we assessed the effect of exposure to environmental enrichment (EE). Remarkably, our results demonstrate an age-dependent modulation of promoter interactions and expression with EE, with aging-like changes induced in young mice upon EE, likely associated with brain maturation, while age-related alterations were reverted in old mice, leading to a partial rejuvenation of aged mouse hippocampi. These findings reveal a dynamic behavior of the neuronal 3D chromatin structure over time, which can be modulated by external interventions.

INTRODUCTION

Aging is a multifactorial biological process characterized by a progressive decline in physiological and cellular functions as a result of molecular alterations accumulated throughout the lifespan.[1,2] This complex process is associated with an increased risk of age-related disorders, such as cancer, cardiovascular diseases, or neurodegenerative disorders.[1] In the last years, several molecular bases of aging have been described. Epigenetic mechanisms, defined as reversible heritable mechanisms that do not change the underlying DNA sequence, play a significant role in the aging process as well as in aging-associated diseases.[1,3–5] The effect of aging on various brain regions has been extensively studied at different molecular levels and especially in the hippocampus, which is crucial for cognition and memory and has active neurogenesis in adults.[6,7] Epigenetic and chromatin alterations in hippocampal cells during aging have been related to cognitive decline[6,8] and associated with neurodegenerative diseases.[9] Moreover, these epigenetic mechanisms can be modulated by environmental factors, ultimately impacting gene expression patterns.[10–12] Nowadays, epigenetic regulation is known to play a critical role in cognition[13] and memory,[14] neurogenesis,[15,16] neuronal plasticity,[17] and neurodegeneration,[18] many of which are affected by aging, stress, and environmental factors.[15,19]

Some of the mechanisms involved in epigenetic regulation are those related to chromatin conformation. Chromatin presents a complex three-dimensional (3D) organization that plays an

This is an open access article under the CC BY-NC license (http://creativecommons.org/licenses/by-nc/4.0/).

important role in the regulation of gene expression[20,21] and the determination of cell identity.[22] The regulatory activity of certain genomic elements, such as enhancers, is essentially controlled by the chromosomal structure. Enhancers, which are modulators of gene expression often located at a long linear distance from the gene, exert their regulatory function through spatial proximity to target gene promoters. These physical interactions are established by the 3D folding of chromatin into loops.[23–26] There are two types of chromatin loops, structural loops and functional loops, the latter being determined by those promoter-enhancer interactions.[27] Furthermore, cell-type-specific expression patterns are determined by the combined effects of proximal and distal regulatory elements.[20]

Chromatin Conformation Capture (3C) technologies have been essential for the study of chromatin organization. Among them, the High-throughput Chromosome Conformation Capture (Hi-C) technique allows for the identification of genome-wide interactions[27] and facilitates the exploration of the 3D genome at different scales, including both chromatin interactions in *cis* (within a chromosome) and in *trans* (between chromosomes).[23,28] Hi-C techniques have provided valuable insights into mechanisms underlying cognition and memory,[29–31] brain development,[32,33] and neurogenesis[34] as well as neuropsychiatric and neurodegenerative disorders.[35,36] Furthermore, variants of the Hi-C technique have been performed to explore cerebellar aging.[37] However, due to the high cost and low resolution of the Hi-C technique, capture Hi-C (CHi-C) approaches have been developed to enrich the sample library in specific genomic regions.[38] One such method is promoter CHi-C (PCHi-C), which enriches the library for promoter interactions using probes that hybridize with promoter fragments.[39] Among other findings, PCHi-C has provided insights into the mechanisms underlying neurodevelopmental diseases[40] and neuropsychiatric disorders.[41] However, the characterization of aging-related alterations in promoter interactions using PCHi-C approaches remains limited.

Chromosomal organization varies greatly across different cell types, resulting in highly cell-type-specific chromatin interactions.[33,42] There is a significant cellular heterogeneity in the brain, neurons and glial cells being the predominant categories.[43] For that reason, different strategies have been employed to mitigate cellular heterogeneity for Hi-C analysis in the brain, including cell sorting.[33,44] However, the starting number of cells is a limitation of PCHi-C, which requires millions of cells; the low-input CHi-C (liCHi-C) method is an alternative suitable for the analysis of very low cell numbers.[45]

Before this study, the influence of age on the environmental effects in the neuronal 3D chromatin interactome was unknown. Therefore, here, we aimed to characterize the 3D chromatin interactome in hippocampal neurons of young and old mice and its association with gene expression to identify functional alterations that occur with age. Furthermore, we investigated the potential of external factors to modify chromatin contacts and gene expression. To achieve this, we exposed young and old mice to environmental enrichment (EE), using an established cognitive and physical enrichment design,[46–49] and we focused on the dorsal hippocampus, due to its involvement in learning and memory as well as cognitive decline with aging.[6] Thus, with our approach, we have characterized alterations in promoter interaction associated with gene expression changes in the context of aging. In addition, we observed an age-dependent impact of EE, where some age-related alterations are boosted by EE in young mice, while others are partially reversed in aged hippocampi.

RESULTS

The 3D chromatin interactome changes with age

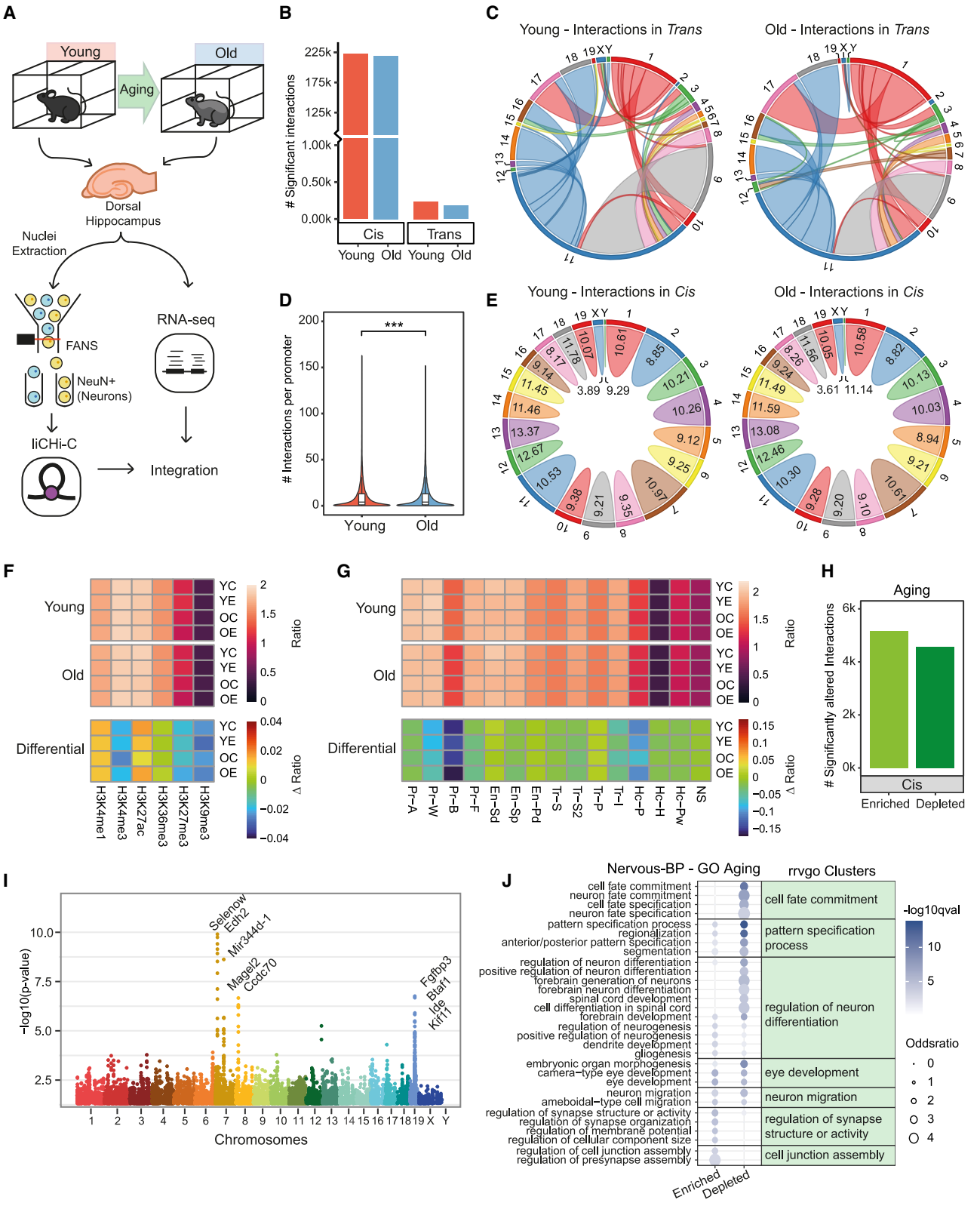
To characterize the 3D chromatin structure in mouse dorsal hippocampal neurons and investigate how is it affected by age, we used a Hi-C approach. First, we purified neuronal nuclei from young and old mouse hippocampi using the well-established intracellular marker NeuN,[50] and subsequently, we performed liCHi-C (Figure 1A).

For liCHi-C, we isolated neuronal nuclei from young and old mouse brains using fluorescence-activated nucleus sorting (FANS) (Figure S1A). Mature $NeuN^+$ neurons comprised approximately 60% of the hippocampal population (Figure S1B). Three biological replicates were performed, each using 1 million neuronal nuclei pooled from three individual mice. liCHi-C libraries were then prepared and deep sequenced. Paired-end reads were processed, mapped, and filtered using the HiCUP pipeline.[52] The percentage of valid reads (mean = 64.336%, SD = 2.416%), the capture efficiency (mean = 60.328%, SD = 3.251%), and the proportion of interactions in *cis* and in *trans* (*trans* mean = 14.882%, SD = 0.362%) revealed no significant differences between replicates of young and old mice (Figures S1C and S1D; Table S1) and demonstrated the high quality of the liCHi-C libraries. Subsequently, the CHiCAGO pipeline[53] was used for significant interaction calling (CHiCAGO score $\geq$5), detecting more than 200,000 significant contacts in merged samples (mean = 221,560, SD = 1,966). The proportion of promoter-promoter interactions remained consistent among replicates, representing around 14.4% of all interactions compared to promoter-to-non-promoter interactions (Figures S1E and S1F; Table S1).

From CHiCAGO interaction calling, we identified 239 CHiCAGO significant contacts in *trans* for young mice, while there were 181 for old mice. For instance, interactions between chromosomes 11 and 9 seemed to be reduced in older mice (Figures 1B, 1C, and S1G). In contrast, both young and old mice displayed over 200,000 CHiCAGO significant contacts in *cis* (222,484 in young and 219,779 in old) (Figure 1B). At a global level, the number of *cis* contacts per promoter was significantly lower in older mice than in younger mice (Wilcoxon $p < 0.001$), and chromosome 13 harbored the highest number of interactions in *cis* per captured promoter in each condition (Figures 1D and 1E). Moreover, the distance distribution of *cis* interactions differed between age groups, as young mice exhibited a significantly greater median distance (263 kb) between interacting regions compared to old mice (254 kb) (Wilcoxon $p < 0.001$) (Figure S1H; Table S1).

Due to their abundance and potential functional implications, we focused on *cis* interactions, performing an integration with histone modifications/chromatin states obtained from mouse hippocampus.[51] Within *cis*-interacting regions, we observed an

CellPress
OPEN ACCESS



(legend on next page)

enrichment of activating histone modifications (e.g., H3K4me3 and H3K27ac) in both young and old mice. However, with aging, we observed certain trends, including a slight decrease in H3K4me3 mark as well as in repressive marks (e.g., H3K9me3) (Figure 1F). Additionally, *cis* interactions were enriched for chromatin states related to promoters and enhancers, but not heterochromatin states. Comparing the two age groups, we found a decrease in the enrichment of some chromatin states with aging. These included bivalent and weak promoters and polycomb-associated heterochromatin (Figure 1G). We have previously described a genome-wide reduction of bivalent domains (regions marked with both H3K4me3 and H3K27me3) with aging.[51] Here, we observed a reduction of interactions with bivalent promoters upon aging, supporting the idea that bivalent domains are highly affected by the aging process.[54]

We next performed a differential analysis using the Chicdiff pipeline,[55] which identifies significant changes in promoter interactions between conditions by pooling interaction counts from contiguous fragments to improve the statistical power. This analysis revealed 9,740 interactions that changed with age ($p < 0.05$), 5,162 interactions showing significant enrichment, and 4,578 interactions showing significant depletion (Figure 1H; Table S2).

Regarding their genomic location, some of the interactions that were most significantly altered with age clustered within specific regions, such as those in chromosome 7 (involving the *Selenow* and *Edh2* promoters) or in chromosome 19 (involving the *Fgfbp3*, *Btaf1*, *Ide*, and *Kif11* promoters) (Figure 1I). Furthermore, Gene Ontology (GO) analysis of promoters with enriched interactions in old mice revealed an association with synapse organization and transcription initiation processes (Figures 1J and S1I; Table S3), suggesting a possible role in synaptic plasticity during aging.[56] Conversely, genes with depleted interactions in old mice were mainly linked to functions like cell fate commitment, pattern specification, and neuron differentiation (Figures 1J and S1I; Table S3), indicating a potential role in cell identity.[41] These results suggest that age-related changes in chromatin interactions are not random but potentially influence the regulation of specific biological pathways.

Transcriptomic analysis reveals age-related changes and potential chromatin interactome link

To assess the impact of aging on the transcriptome and its potential connection to the chromatin interactome, we performed RNA sequencing (RNA-seq) on dorsal hippocampus tissue from mice (Table S4). Since sorting NeuN$^+$ cells from the dorsal hippocampus requires membrane permeabilization for labeling this intracellular marker, resulting in the loss of mRNA molecules, RNA-seq was performed using bulk hippocampal cells, following previous experimental designs.[30] Subsequent integration with liCHi-C data allowed us to describe changes in promoter interactions with a possible influence on gene expression regulation (Figure 1A).

Principal-component analysis (PCA) of gene expression shows a segregation of samples by age (Figure 2A). Differential expression analysis identified genes whose expression levels were significantly altered with aging. Specifically, we found 806 genes significantly upregulated, while 1,286 genes were significantly downregulated with age (Figures 2B; Table S5). To explore the functional implications of these age-related gene expression changes, we performed a gene set enrichment analysis (GSEA)[57] on expression data. This analysis identified 68 gene sets significantly downregulated with aging. Many of these downregulated gene sets were associated with telencephalon cells and collagen formation processes (Figure 2C; Table S6). Conversely, 26 gene sets exhibited significant upregulation in aged mice. These upregulated sets included those related to neuron markers and neurotransmitters (Figure 2C; Table S6).

We next explored the functional implications of the age-related alterations in chromatin interactions. The relationship

Figure 1. Promoter interactions of young and old mouse hippocampal neurons and their change with aging

(A) Schematic of the study design for young and old mouse conditions, using low-input promoter capture Hi-C (liCHi-C) and RNA-seq analysis and performing integrative analysis.

(B) Bar plot illustrating the total number of CHiCAGO significant interactions in *trans* and in *cis* for young and old mice. k, 1,000.

(C) Chord plots representing the *trans* interaction proportion of each mouse chromosome (outside number) for young mice (left) and old mice (right).

(D) Violin plots showing the number of interactions per promoter. Merged samples for young and old conditions are represented. Wilcoxon signed-sum test for paired samples was used to compare groups ($p = 1.331e{-}07$). ***$p < 0.001$.

(E) Chord plots representing the *cis* interaction of each mouse chromosome (outside number) for young mice (left) and old mice (right). The width of each chord represents the proportion of *cis* interactions of each chromosome, and the inside numbers indicate the average number of *cis* interactions per captured promoter in each chromosome.

(F and G) Heatmaps representing histone mark (F) and chromatin state (G) enrichment analysis of significant interactions in *cis* for young and old mice. Six common histone posttranslational modifications and the 15 chromatin states (see STAR Methods) defined by histone marks from four mouse hippocampus datasets of a previous study[51] (corresponding to the four experimental conditions of the study: YC, young control; YE, young with environmental enrichment; OC, old control; OE, old with environmental enrichment) were used in the enrichment analysis. First color scale (on top) represents the magnitude of enrichment (ratio); ratios were calculated by comparing significant interaction overlaps and random sampling overlaps. Second color scale (on bottom) reflects the differential ratio (Δ ratio) with aging (old vs. young), calculated by subtracting the young mouse values from the old mouse values.

(H) Bar plot illustrating the total number of Chicdiff interactions in *cis* that change significantly ($p < 0.05$) with aging, distinguishing between enriched and depleted interactions. k, 1,000. Also see Table S2.

(I) Manhattan plot of differential interactions in *cis* with aging (Chicdiff $p < 0.05$).

(J) Bubble plot representing Gene Ontology (GO) term enrichment based on nervous system-associated biological processes (Nervous-BP) for promoter genes with significantly enriched and depleted interactions ($p < 0.05$) with aging (see Table S3). Bubble color intensity represents the statistical significance ($-\log_{10} q$ value), and dot size reflects odds ratio. Top significant GO terms were grouped following rrvgo clustering and are named by the most representative term of the group.

Also see Figure S1 and Table S1.

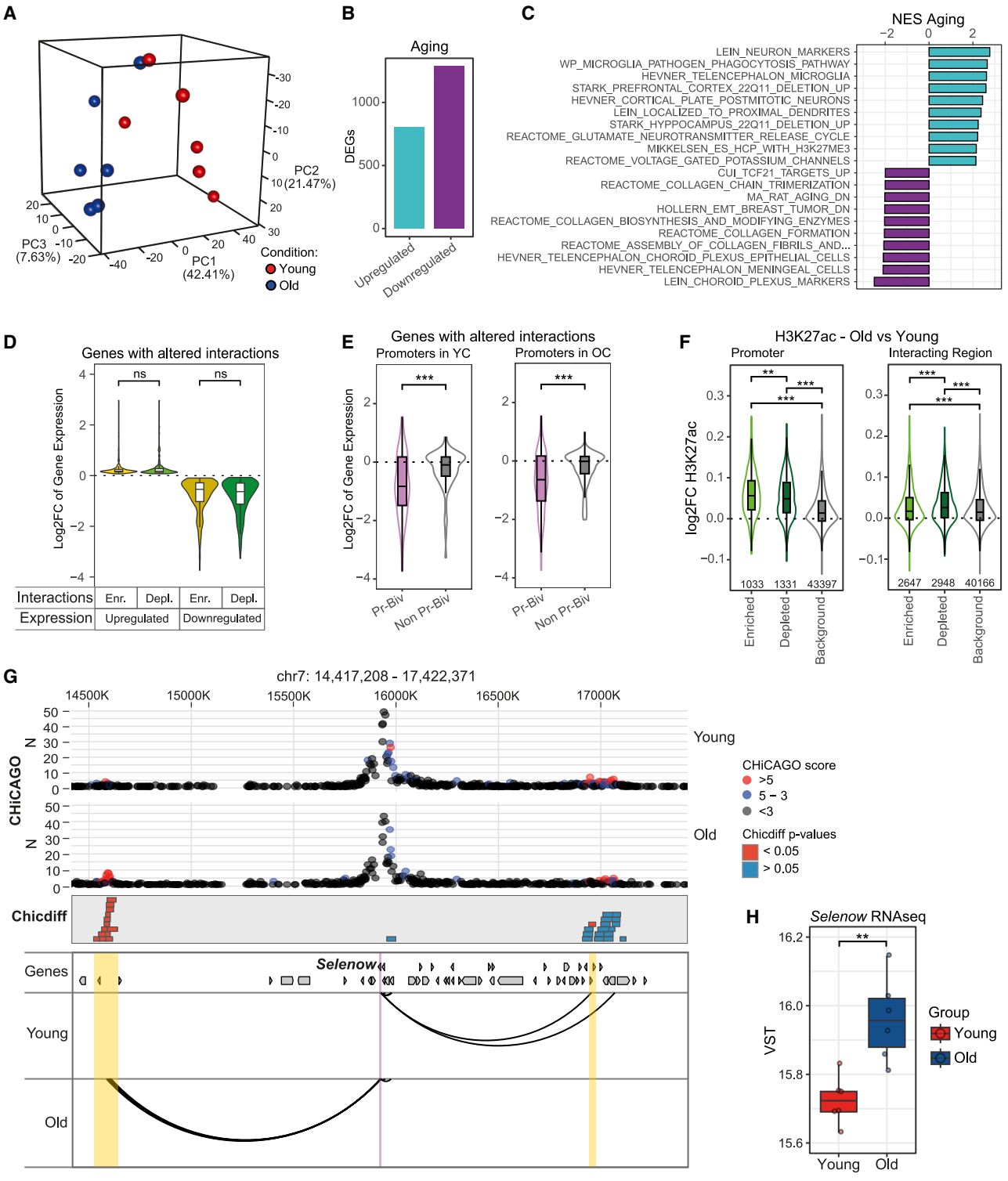


Figure 2. Gene expression alterations with aging and functional implications of promoter interactions

(A) Principal-component analysis (PCA) for the 2,000 most variable genes of RNA-seq replicates in young and old conditions. The proportion of variance explained for the PC1, PC2, and PC3 components is indicated.

(B) Bar plot illustrating the number of differentially expressed genes (DEGs) with aging (old vs. young), distinguishing between upregulated and downregulated genes (adj. $p < 0.05$). Also see Table S5.

(legend continued on next page)

between promoter interactions and transcription is complex, convoluted by multiple layers of regulation (e.g., chromatin state, transcription factor binding, histone modifications, RNA processing, and non-coding RNAs),[42,58] making it difficult to draw direct correlations (Figure 2D). However, for genes with bivalent promoters showing significant interaction alterations, expression was significantly downregulated with age (Figure 2E). This was accompanied by an increase in the total number of bivalent promoters detected in aged mice (Figure S2A). Bivalent promoters, which are promoters marked by both active and repressive histone marks, are crucial regulatory elements in neurodevelopment and plasticity.[59] Under this complex regulatory landscape, modest correlation between promoter interactions and gene expression can be biologically meaningful and underscores the need for integrative analysis of multiple layers of regulation.[40] Moreover, we explored other layers of regulation and found that significantly altered interactions were associated with an increase of H3K27ac in promoter regions (Figure 2F), as well as that of other active histone marks (Figures S2B–S2D), while repressive marks (e.g., H3K27me3 or H3K9me3) did not exhibit significant changes in promoters (Figures S2E and S2F). Furthermore, in the interacting regions of significantly altered contacts, similar, though slighter, observations were detected (Figures S2B–S2F).

By integrating these molecular layers, we identified several genes with significant changes in both promoter interactions and gene expression with age, such as *Selenow* or *Kif11*, which exhibit some of the most significant changes in promoter interactions (Figure 1I). For instance, the *Kif11* gene, which seems to be involved in synaptic regulation[60] and neuronal migration,[61] shows increased promoter contacts with age (Figure S3A), even though its expression is downregulated with aging (Figure S3B). On the other hand, the *Selenow* gene has been involved in neuroprotection against oxidative stress[62,63] as well as memory formation[64] and inhibition of tau protein aggregation.[65,66] At the promoter interactome level, *Selenow* exhibited an age-associated decrease in interactions within a region downstream, with an accompanying increase in interactions (Chicdiff p of eight interacting regions < 0.0000001) within a specific genomic region of chromosome 7 (chr7:14,522,438—14,639,621) (Figure 2G; Table S7). This implies that, with age, a loop is generated between the *Selenow* promoter and this specific region. Moreover, RNA-seq analysis revealed a significant upregulation of *Selenow* expression in older mice (adj. p = 0.012; log2 fold change [LFC] = 0.646) (Figure 2H). Taken together, these results suggest that the age-related upregulation of *Selenow* expression might be influenced by the chromatin reorganization and formation of a chromatin loop.

EE has an age-dependent impact on the chromatin interactome

To investigate whether external stimuli may influence and modulate chromatin interactions, we explored the impact of EE on promoter interactions. First, we analyzed the impact of EE within each age group, distinguishing between EE in young mice (YEE vs. young control) and EE in old mice (OEE vs. old control) (Figure 3A). liCHi-C experiments were performed on samples from EE mice, and sequencing data were processed identical to the control samples. No significant differences were observed between the replicates for both control and EE samples using HiCUP and CHiCAGO statistics. This included the percentage of captured valid reads, the *cis-trans* proportions, the number of CHiCAGO significant interactions, and the promoter-promoter interactions proportion (Figures S1C–S1F and S4A–S4D; Table S1).

We analyzed the number of significant interactions in *trans* and *cis* for YEE and OEE mice. For interactions in *trans*, we identified 241 CHiCAGO significant contacts in YEE mice and 245 in OEE mice (Figure 3B). Furthermore, YEE and OEE mice exhibited distinct patterns compared to their respective control conditions. For example, we observed a higher number of interactions between chromosomes 11 and 17 in YEE and an increase in interactions between chromosomes 5 and 8 in OEE (Figures 1C, 3C, S1G, and S4E). The total number of significant *cis* interactions also remained comparable, with over 200,000 identified in both YEE (218,633) and OEE (215,871) mice (Figure 3B), with median linear distances of 263 and 250 kb, respectively, and with the distance distribution between

(C) Bar plots reflecting the normalized enrichment score (NES) of GSEA gene sets from the M2 collection (MSigDB). Gene set NESs were calculated for aging (old vs. young). Top significantly enriched (teal) and depleted (purple) gene sets are shown (false discovery rate [FDR] q < 0.05). Extended lists of significant gene sets are available in Table S6.

(D) Violin plots showing the $\log_2$ fold change of genes with significantly altered interactions, splitting between genes upregulated or downregulated with aging (p < 0.05) and comparing those with enriched or depleted interactions (p < 0.05) with aging. Significance was calculated with the Wilcoxon rank-sum test.

(E) Violin plots showing the $\log_2$ fold change of genes (p < 0.05) with significantly altered interactions (p < 0.05) with aging, distinguishing between genes with bivalent promoters (Pr-Biv) and without bivalent promoters (Non Pr-Biv), obtained from young control (YC) and old control (OC) datasets of a previous study.[51] Significance was calculated with the Wilcoxon rank-sum test.

(F) Violin plots showing the differential ($\log_2$ fold change) with aging (old vs. young) of histone mark H3K27ac from a previous study.[51] H3K27ac peaks were analyzed at promoter regions and interacting regions, differentiating between peaks associated with significantly enriched interactions (p < 0.05), with significantly depleted interactions (p < 0.05), and with non-significantly altered interactions (p > 0.05; background). Sample sizes are shown inside the plots. Significance was calculated with the Wilcoxon rank-sum test.

(G) *Selenow* promoter-centered interactions according to liCHi-C data in young and old conditions. Top: dots represent counts of contacts, highlighting the CHiCAGO significant ones in red. Rectangles indicate significantly altered interactions (p value) between conditions based on Chicdiff analysis. Bottom: arcs represent CHiCAGO significant contacts. Purple shade depicts *Selenow* gene promoter and yellow shade depicts regions with significantly altered interactions (see also Table S7). Arrows symbolize gene placement and orientation along the genomic window.

(H) Boxplots indicating the RNA-seq expression measurements (variance-stabilizing transformed [VST] data) for the *Selenow* gene across young and old mice (**adj. p < 0.01). The median scores for each condition are indicated. Boxes represent the interquartile range (IQR), and whiskers extend to the most extreme data points within 1.5 × IQR. Dots denote individual mouse data.

^{ns}p > 0.05, $^{*}p$ < 0.05, $^{**}p$ < 0.01, and $^{***}p$ < 0.001. Also see Figures S2 and S3.

CellPress
OPEN ACCESS

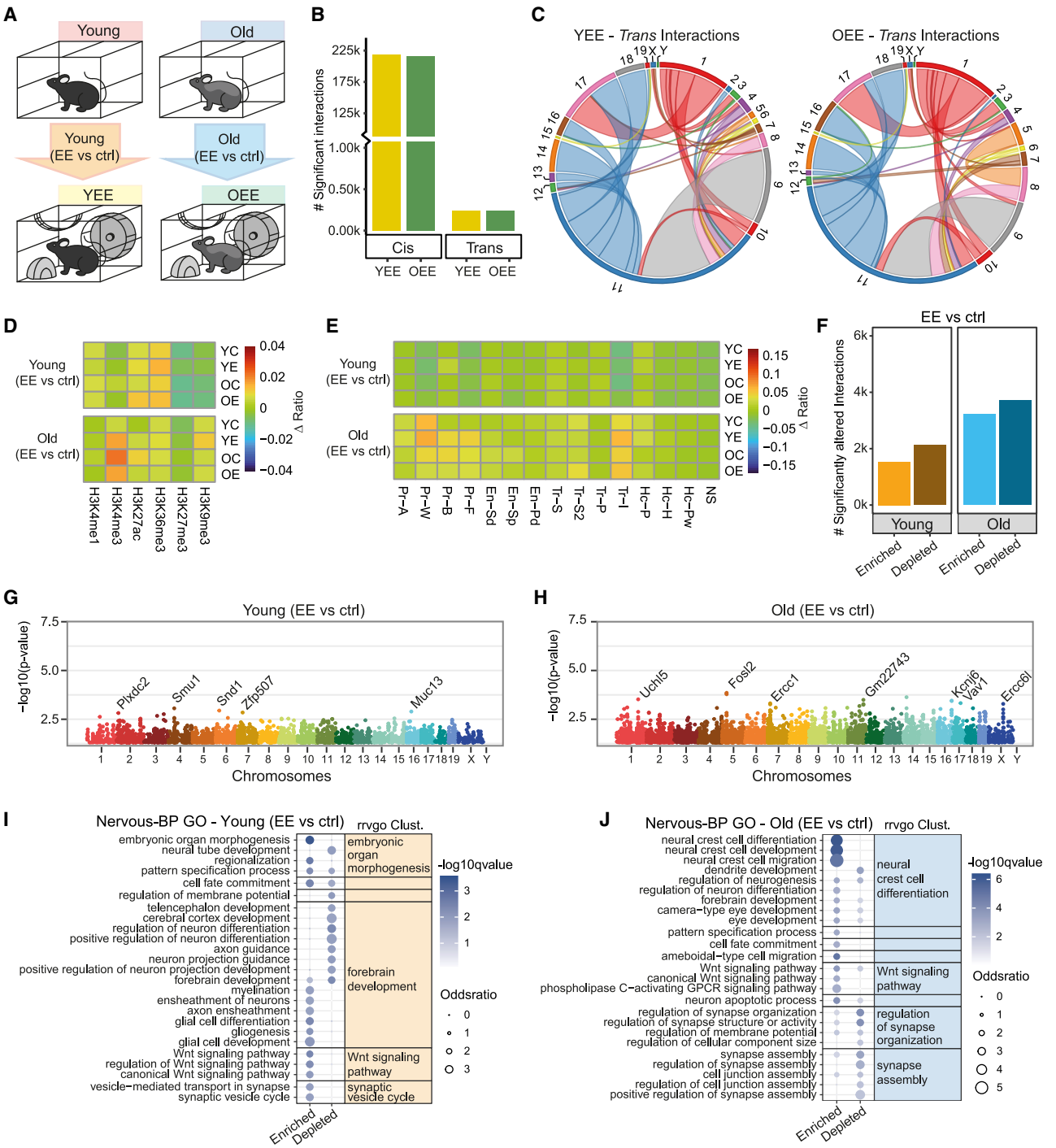


Figure 3. Promoter interaction alterations with environmental enrichment in young mice and in old mice

(A) Schematic of the environmental enrichment (EE) design. We distinguish between the exposures to EE in young mice (EE in young), comparing young control mice with young mice with EE (YEE), and the exposures to EE in old mice (EE in old), comparing old control mice with old mice with EE (OEE).

(B) Bar plot illustrating the total number of CHiCAGO significant interactions in *trans* and in *cis* for YEE and OEE mice. k, 1,000.

(C) Chord plots representing the *trans* interaction proportion of each mouse chromosome (outside number) for young mice (left) and old mice (right).

(D and E) Heatmaps representing histone mark (D) and chromatin state (E) enrichment analysis of significant interactions in *cis*. Color scale reflects the differential ratio (Δ ratio) with EE in young mice (top) and in old mice (bottom), and it was calculated by subtracting the control condition values from the EE condition values.

(legend continued on next page)

OEE and old control conditions being significantly different (Wilcoxon $p < 0.001$) (Figure S4F). However, the number of *cis* contacts per promoter was significantly lower in EE conditions (YEE and OEE) than in their corresponding control conditions (Figure S4G), which was also evident when exploring chromosomes individually (Figures 1E and S4H). Thus, exposure to EE revealed promoter interaction alterations in *cis* but also in *trans* interactions.

Subsequently, we conducted histone and chromatin state enrichment analysis within *cis*-interacting regions for EE conditions, and we compared them with control conditions. While histone modifications exhibited minor variations in response to EE (Figure 3D), we did observe slight changes in specific chromatin states (Figure 3E). Interestingly, the enrichments for weak promoter and transcription initiation states exhibited opposing trends in young and old mice with EE. With EE in young mice, these states showed a slight decrease in enrichment, mirroring the trend observed with aging. Conversely, with EE in old mice, the enrichment for these states increased slightly (Figure 3E).

Differential analysis using Chicdiff revealed distinct patterns of interaction alterations upon EE (Figure 3F). With EE in young mice, we observed a higher number of significantly depleted interactions (2,116) compared to enriched interactions (1,531) (Figure 3F; Table S2), including, for instance, *Smu1* and *Snd1* promoter interactions (Figure 3G). Similarly, with EE in old mice, we identified more depleted interactions (3,706) than enriched interactions (3,212) (Figure 3F; Table S2). These altered interactions involved *Fosl2* and *Uchl5* promoters (Figure 3H). Notably, there were fewer significantly altered interactions observed under EE conditions compared to what we observed with aging (almost 10,000 changes; Figure 1H). This suggests that aging had a stronger impact on the chromatin interactome than EE, at least on hippocampal neurons.

GO analysis of gene promoters with altered interactions upon EE revealed several genes that were associated with different biological processes in young and old mice. Some processes, such as Wnt signaling, were mainly associated with enriched interactions with EE in both young and old mice. However, other processes seemed to be associated with depleted interactions with EE in young mice but with enriched interactions with EE in old mice, e.g., processes related to nervous system development and differentiation (Figures 3I, 3J, S4I, and S4J; Table S3). Altered interactions with EE in old mice were also related to regulation of neurogenesis and synapse organization, which aligns with known mechanisms of neuronal plasticity.[67] Taken together, all these findings suggest that EE has a differential effect on chromatin contacts in young and old mice.

The age-dependent effect of EE on chromatin interactions is recapitulated at the transcriptional level

PCA of transcriptomic data of the entire hippocampus represents the variability at the gene expression level among control and EE conditions. Notably, old and young EE conditions cluster closely in the PCA (Figure 4A). Differential expression analysis identified a higher number of differentially expressed genes (DEGs; adj. $p < 0.05$) upregulated (409) or downregulated (460) with EE in young mice compared to the old mice (9 upregulated, 15 downregulated). Notably, most genes were specific to either EE in young or EE in old mice, even under an unadjusted significance level (Figures 4B and S5A; Table S5). Moreover, while GSEA revealed a general/common effect of EE in pathways associated with choroid plexus, it also showed an age-dependent effect of EE on some pathways, such as those related with midbrain markers or promoters with H3K27me3 in brain (Figure 4C; Table S6). Taken together, these findings suggest that, similar to the chromatin interactome, the impact of EE on gene expression is influenced by the age of the organism, with more DEGs in young than in old mice.

The integration of chromatin interactions and gene expression revealed results similar to what was described in aging analysis. Although, in general terms, there is not a clear pattern in the transcriptome outcome (Figure 4D), genes with bivalent promoters showing significant interaction changes were significantly affected by EE (Figure 4E). With EE in young mice, genes with bivalent promoters were significantly downregulated compared to non-bivalent genes, similar to what was observed with aging, while with EE in old mice, they were significantly upregulated, in contrast to what we observed in young and aging mice (Figure 4F). Interestingly, the total number of bivalent promoters increased with EE in young mice, approaching the levels of old mice, whereas with EE in old mice, values comparable to those found in young mice were recovered (Figure S5B). Furthermore, significantly altered interactions with EE were associated with changes on active histone marks in promoters. Remarkably, with EE in young mice, H3K27ac and other active histone marks followed the same trend observed with aging, while with EE in old mice, they had a trend opposite to the finding in aging (Figures 4F and S5C–S5G). Moreover, in the interacting regions, similar but slighter tendencies were observed (Figures 4G and S5C–S5G).

One example of a gene with significant changes in promoter interactions with EE in young mice was *Xbp1*, which plays a role in cognition and behavior.[68] *Xbp1* showed significant increase in promoter interactions with EE in young mice (Figure S7A; Table S7), accompanied by a decrease in expression (Figure S7B). Conversely, *Sema5b*, a gene involved in axon growth and reduction of synapse connections,[69] showed

Six common histone posttranslational modifications and the 15 chromatin states (see STAR Methods) defined by histone marks from four mouse hippocampus datasets (the four experimental conditions: YC, YE, OC, and OE) of a previous study[51] were used in the enrichment analysis.

(F) Bar plot illustrating the total number of Chicdiff interactions in *cis* that change significantly ($p < 0.05$) with the EE in both young and old mice, distinguishing between enriched and depleted interactions. k, 1,000. Also see Table S2.

(G and H) Manhattan plots of differential interactions in *cis* (Chicdiff $p < 0.05$) with EE in young mice (G) and EE in old mice (H).

(I and J) Bubble plots represent Gene Ontology (GO) term enrichment based on nervous system-associated biological processes (Nervous-BP) for promoter genes with significantly enriched or depleted interactions ($p < 0.05$) with EE in young mice (I) and in old mice (J) (see Table S3). Bubble color intensity represents the statistical significance ($-\log_{10} q$ value), and dot size reflects odds ratio. Top significant GO terms were grouped following rrvgo clustering, which are named by the most representative term of the group. Also see Figure S4.

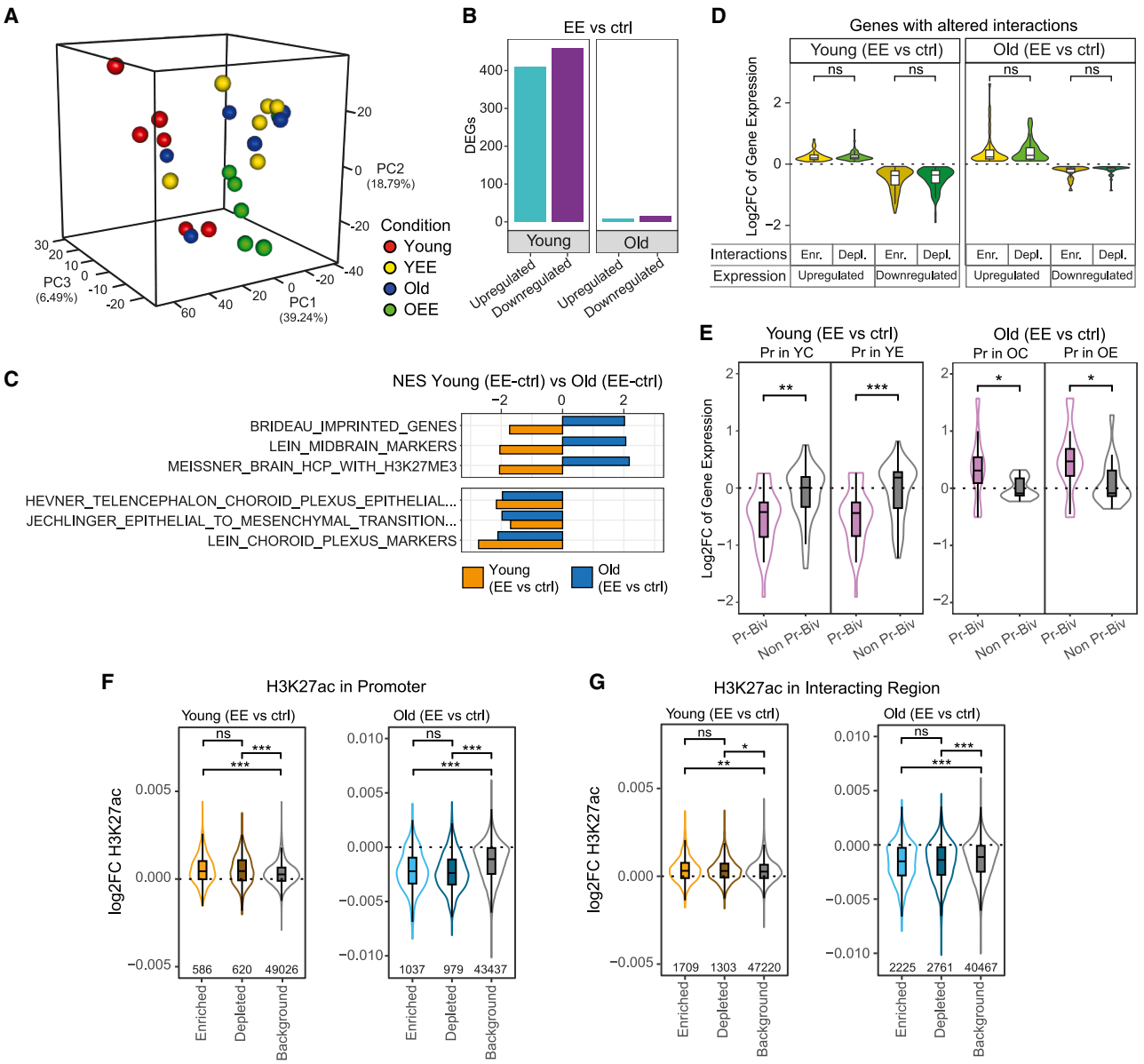


Figure 4. Effects of environmental enrichment at RNA level and the functional implications of promoter interactions

(A) Principal-component analysis (PCA) for the 2,000 most variable genes of RNA-seq replicates in young, old, YEE, and OEE conditions. The proportion of variance explained for the PC1, PC2, and PC3 components is indicated.

(B) Bar plot illustrating the number of differentially expressed genes (DEGs) (adj. $p < 0.05$) with EE in young mice (left) and EE in old mice (right), distinguishing between upregulated and downregulated genes. Also see Table S5.

(C) Bar plots reflecting the normalized enrichment score (NES) of GSEA gene sets from the M2 collection (MSigDB). Gene set NESs for EE in young mice and EE in old mice are shown (FDR $q < 0.05$). Also see Table S6.

(D) Violin plots showing the $\log_2$ fold change of genes with altered interactions in response to EE in young mice (left) and in old mice (right). Upregulated and downregulated genes with EE ($p < 0.05$) are represented separately, comparing those with significantly enriched or depleted interactions with EE ($p < 0.05$). Significance was calculated with the Wilcoxon rank-sum test.

(E) Violin plots showing the $\log_2$ fold change of genes ($p < 0.05$) with significantly altered interactions ($p < 0.05$) in response to EE in young mice (left) and in old mice (right), distinguishing between genes with bivalent promoters (Pr-Biv) and without bivalent promoters (Non Pr-Biv), obtained from young control (YC), old control (OC), young EE (YE), and old EE (OE) datasets of a previous study.[51] Significance was calculated with the Wilcoxon rank-sum test.

(F and G) Violin plots showing the differential ($\log_2$ fold change) at promoter regions (F) or interacting regions (G) of histone mark H3K27ac from a previous study.[51] H3K27ac peaks were analyzed for EE in young and EE in old mice, differentiating between peaks associated with significantly enriched interactions ($p < 0.05$), with significantly depleted interactions ($p < 0.05$), and with non-significantly altered interactions ($p > 0.05$; background). Sample sizes are shown inside the plots. Significance was calculated with the Wilcoxon rank-sum test.

$^{ns}p > 0.05$, $^{*}p < 0.05$, $^{**}p < 0.01$, and $^{***}p < 0.001$. Also see Figures S5, S6, and S7.

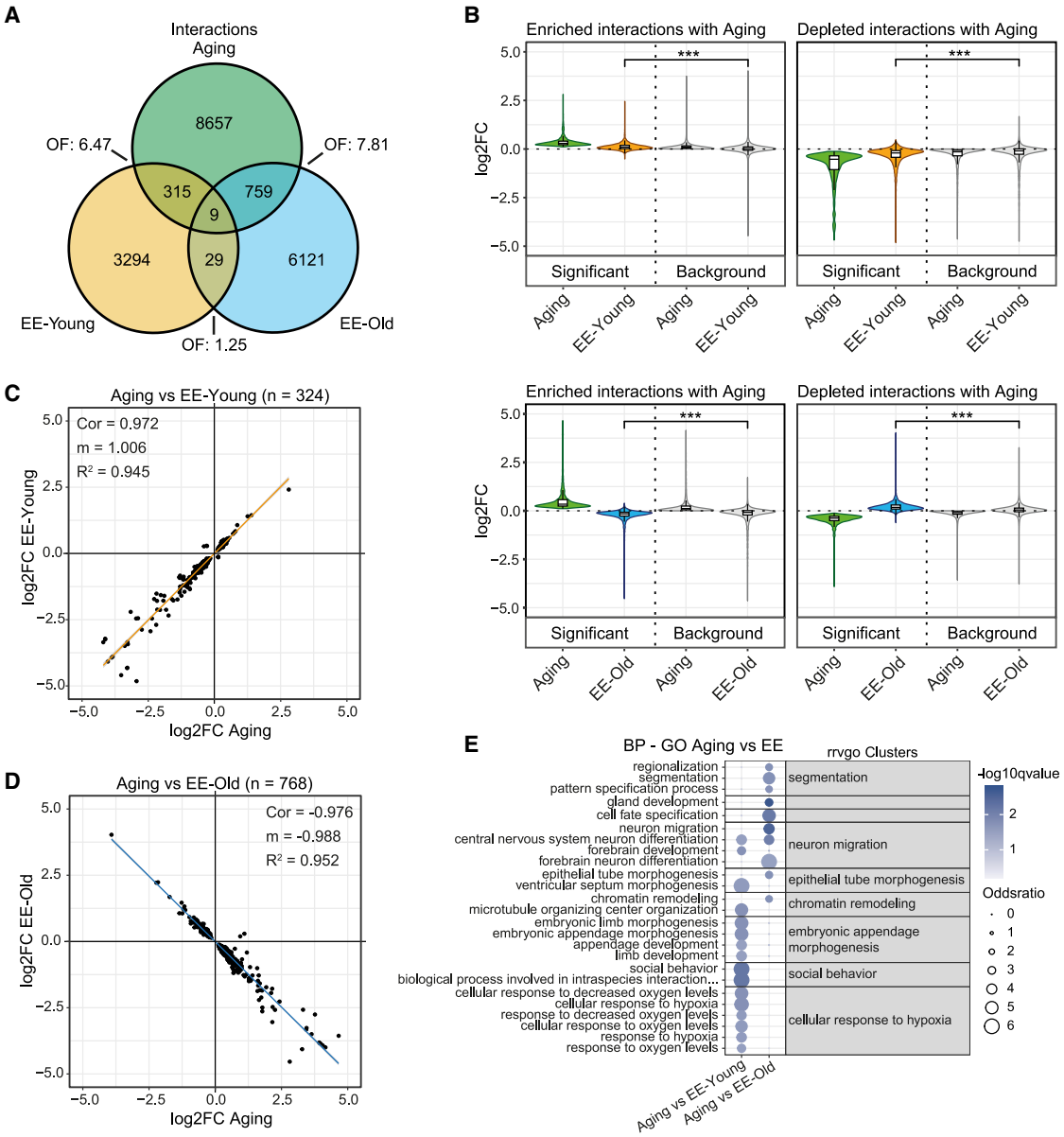


Figure 5. Comparative analysis between aging and environmental enrichment in both young and old mice at the promoter chromatin interactome level

(A) Venn diagram depicting the number of significant interactions ($p < 0.05$) for aging (green), EE in young mice (orange), and EE in old mice (blue). The numbers of overlapping interactions are indicated, and their representation/overlapping factor (OF) was calculated using hypergeometric distribution: 6.47 for aging vs. EE-young ($p = 0$; universe [u] = 710,041 interactions), 7.81 for aging vs. EE-old ($p = 1.5e{-}152$; u = 685,339), and 1.25 for EE-young vs. EE-old ($p = 0.103$; u = 827,763).

(B) Violin plots showing the $\log_2$ fold change for promoter interactions under two comparatives: with aging and EE in young mice (top) or with aging and EE in old mice (bottom). Enriched interactions (left) and depleted interactions (right) with aging were represented separately. Interactions significantly altered with aging ($p < 0.05$; significant) were compared to those that were not significantly altered with aging ($p > 0.05$; background). Significance was calculated with the Wilcoxon rank-sum test. ***$p < 0.01$.

(C) Scatterplot indicating a back-to-back comparison of $\log_2$ fold change of significantly altered interactions for aging ($p < 0.05$) and for EE in young mice ($p < 0.05$) (Pearson's correlation score = 0.972; $p < 2.2e{-}16$). Orange line indicates the regression line (slope and R^2 value are shown), and the gray shade represents the confidence interval.

(D) Scatterplot representing a back-to-back comparison of $\log_2$ fold change of significantly altered interactions for aging ($p < 0.05$) and for EE in old mice ($p < 0.05$) (Pearson's correlation score = -0.976; $p < 2.2e{-}16$). Blue line indicates the regression line (slope and R^2 value are shown), and the gray shade represents the confidence interval.

(legend continued on next page)

a significant decrease in its promoter interactions with EE in old mice (Figure S7C; Table S7), accompanied by a decrease in expression (Figure S7D). These findings highlight the age-dependent influence of EE on interactions and expression of specific genes.

Age-associated changes in the chromatin interactome are boosted by EE in young mice and partially reversed by EE in old mice

To explore the relationship between aging and EE, we compared these processes with one another (aging vs. EE in young; aging vs. EE in old). We found that 324 interactions significantly altered with aging also exhibited significant changes with EE in young mice (overlapping factor: 6.47), while 768 of these interactions altered with aging also changed significantly with EE in the old mice (overlapping factor: 7.81) (Figure 5A). This supports the notion that EE has a substantial impact on the age-associated alterations in the chromatin structure in both older and young individuals. Surprisingly, only 38 interactions were shared between EE in young and EE in old (overlapping factor: 1.25), where 9 of them displayed significant changes in all three processes (aging, EE in young, and EE in old) (Figure 5A). These observations demonstrate that the effect of EE depends significantly on the age of the mice, at least at the chromatin structure level.

We performed further analysis focused on interactions that changed significantly with aging, and their fold change with EE revealed distinct patterns depending on the age. In young mice, the direction of change (increase or decrease) in interactions upon EE generally mirrored the change tendency observed with aging (Figures 5B and S8A). However, in old mice, EE induced changes in interactions with the opposite trend compared to those observed with aging (Figures 5B and S8B).

Furthermore, we focused on specific interactions that changed significantly with both aging and EE (Figures 5C and 5D). In young mice, these overlapping changes ($n = 324$) showed a positive correlation (slope = 1.006; $R^2 = 0.945$) (Figure 5C), indicating that EE in young mice partially mimics the age-related trends in chromatin interactions. However, in old mice, the overlapping changes ($n = 768$) exhibited a negative correlation (slope = −0.988; $R^2 = 0.952$) (Figure 5D), demonstrating that EE tends to partially reverse the age-related changes in promoter interactions in old mice.

Then, we observed that the genes with specific interaction alterations for young mice or for old mice were involved in distinct biological processes (Figure 5E). This indicates that those altered interactions are highly age specific. In young mice, those gene promoters with altered interactions upon aging and EE were mainly associated with processes like social behavior, response to hypoxia, and morphogenesis, while those altered in old mice were linked to processes such as segmentation, cell-fate specification, or neuron migration and differentiation (Figure 5E; Table S3). Taken together, our findings highlight the differential effect of EE depending on age, with EE promoting age-related changes in promoter interactions in young mice and partially counteracting aging-related alterations in old mice.

The age-related differential effect of EE on the chromatin interactome is further mirrored at the level of gene expression

To investigate the relationship between aging and EE at the transcriptional level, we conducted the same comparative analysis (aging vs. EE in young; aging vs. EE in old) with RNA-seq data, and we observed similar results compared with interactions (Figure 6A). We found 235 DEGs (1,711 genes with unadj. p value) with aging and EE in young mice (overlapping factor: 2.51) and 6 DEGs (364 genes with unadj. p value) with aging and EE in the old mice (overlapping factor: 2.32), while only 2 DEGs (265 genes with unadj. p value) were shared between EE in young and EE in old (overlapping factor: 1.86) (Figure 6A). These observations indicate that the effect of EE at the gene expression level also depends on the age.

Further analysis that focused on DEGs for aging and EE revealed that gene expression fold changes followed the same trends we observed with chromatin interactions, i.e., in young mice, the direction of change (increase or decrease) in expression upon EE generally followed the tendency observed with aging, while in old mice, EE induced changes with the opposite trend observed with aging (Figures 6B, 6C, and S9A). Moreover, these tendencies were further corroborated by the integrative analysis of promoter interactions and gene expression, obtaining some genes with altered interactions (unadj. $p < 0.05$) with aging and EE, whose gene expression followed the trends described above (overlap for aging vs. EE-young with unadj. $p < 0.05$, 12 genes; overlap for aging vs. EE-old with unadj. $p < 0.05$, 6 genes) (Figure S9B; Table S8). Notably, neuron-derived neurotrophic factor (*Ndnf*) and *Whrn* were the only genes that met the condition of a 0.05 adjusted p value threshold for expression in aging and EE in young mice, while only *P2rx5* met this criterion for aging and EE in old mice (Figure S9B).

GSEA identified several gene sets exhibiting similar modulation with aging and EE in young mice (e.g., neuron markers or telencephalon cells) (Figure 6D; Table S6). Interestingly, comparing aging and EE in old mice revealed gene sets similar to those identified when comparing EE in both young and old mice (Figures 4D and 6E; Table S6). This suggests that some pathways are modulated in the same way by both aging and EE in young mice but are regulated in the opposite direction by EE in old mice. This observation is further supported using GO terms (Figure S9C; Table S6). Additional analysis using the LEIN markers dataset[70] reinforced these observations, where aging and EE in young mice displayed similar patterns, such as the enrichment of neuronal and dendritic markers. In contrast, EE in old mice showed distinct patterns, including an enrichment in brain-region-specific markers that were depleted with aging and EE in young mice (Figure S9D; Table S6).

(E) Bubble plot represents Gene Ontology (GO) term enrichment based on all biological processes (BP) for gene promoters with altered interactions with aging ($p < 0.05$) and EE in young mice ($p < 0.1$) or with aging ($p < 0.05$) and EE in old mice ($p < 0.1$). Less restrictive significances for EE were used to be able to perform the GO analysis. Also see Table S3. Bubble color intensity represents the statistical significance ($-\log_{10} q$ value), and dot size reflects the odds ratio. Top significant GO terms were grouped following rrvgo clustering, which are named by the most representative term of the group. Also see Figure S8.

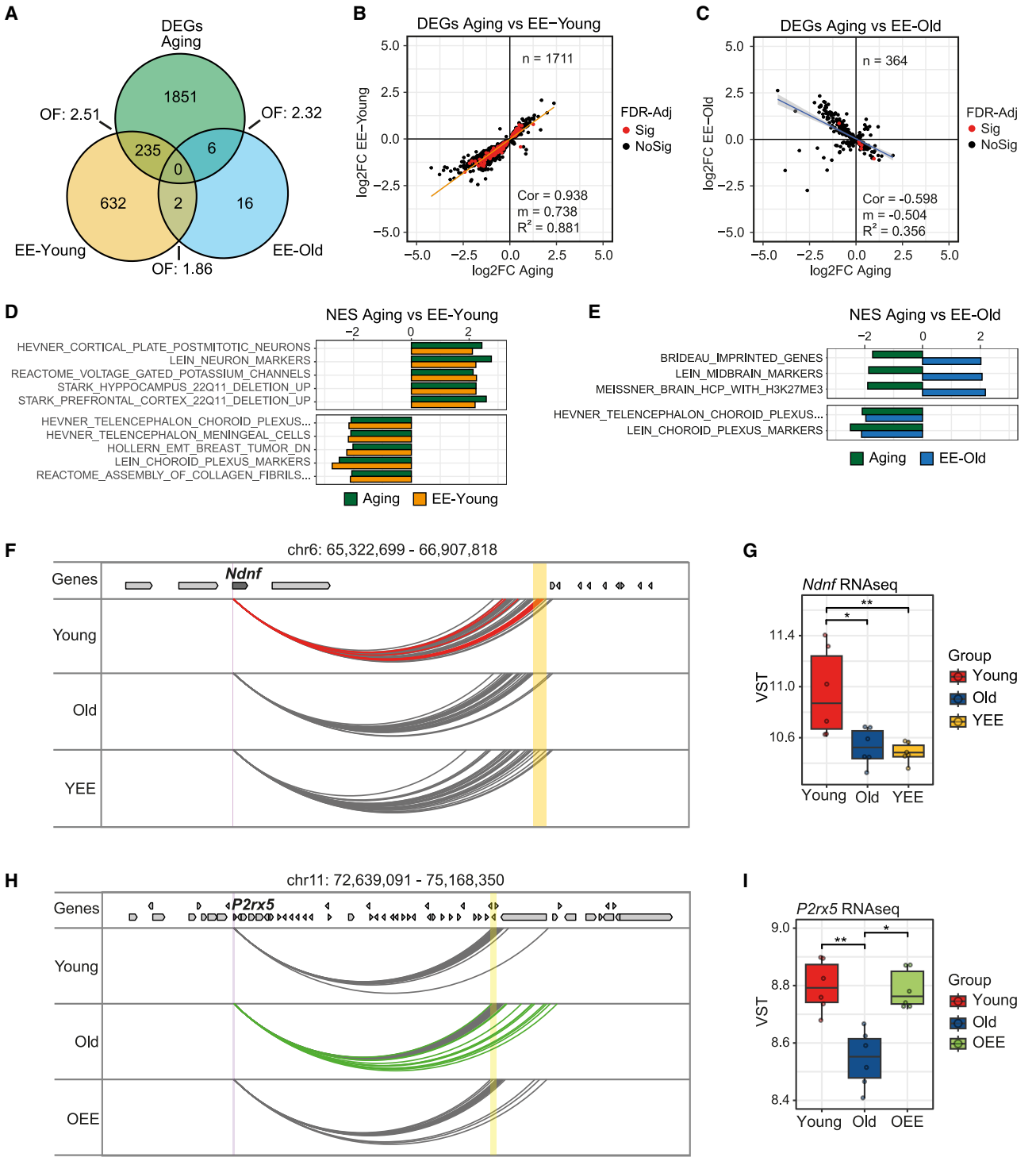


Figure 6. Gene expression differences between aging and environmental enrichment in both young and old mice and integration with promoter interactions

(A) Venn diagram depicting the number of DEGs (adj. $p < 0.05$) with aging (green), EE in young mice (orange), and EE in old mice (blue). The numbers of overlapping DEGs are indicated, and their representation/overlapping factor (OF) was calculated using hypergeometric distribution (universe = 19,388 genes): 2.51 for aging vs. EE-young (p = 6.1e−43), 2.32 for aging vs. EE-old (p = 0.038), and 1.86 for EE-young vs. EE-old (p = 0.292).

(legend continued on next page)

In the comparison of aging and EE in young mice, *Ndnf* emerges as an example of the similar changes at the interaction and expression levels. *Ndnf* is mainly expressed in neurons and promotes neuronal growth, migration, and neurite outgrowth, among others.[71] *Ndnf* promoter interactions decreased with both aging and EE in young mice. Specifically, the most significantly altered interaction for *Ndnf* was reduced with both aging (p = 0.005; LFC = −0.532) and EE in young mice (p = 0.015; LFC = −0.519) (Figure 6F; Table S7). Nonetheless, at the gene expression level, *Ndnf* was downregulated with both aging (adj. p = 0.012; LFC = −0.598) and EE in young mice (adj. p = 0.007; LFC = −0.662) (Figure 6G).

On the other hand, comparing aging and EE in old mice, *P2rx5* exemplifies the observed reversal in interactions and gene expression. *P2rx5* is a purinergic receptor widely expressed in different regions of the central nervous system since embryonic development.[72,73] Some *P2rx5* promoter interactions increased with aging (p = 0.047; LFC = 0.373), while they were reverted with EE in old mice (p = 0.035; LFC = −0.420) (Figure 6H; Table S7). *P2rx5* expression was downregulated during aging (adj. p = 0.001; LFC = −0.907) and upregulated with EE in old mice (adj. p = 0.033; LFC = 0.860) (Figure 6I).

Taken together, our findings reveal an age-dependent effect of EE in hippocampal neurons. In young mice, EE seems to stimulate or promote some age-related changes in the promoter interactome and gene expression, possibly associated with the development or maturation of the hippocampus. Conversely, in old mice, some of the interactome and transcriptome changes identified with aging can be reversed by EE, potentially indicating a partial rejuvenation of the hippocampal neurons.

DISCUSSION

The aging process involves an accumulation of degenerative phenomena due to molecular alterations over time. Here, we used a mouse model comprising both young and old individuals and compared the 3D chromatin interactome in dorsal hippocampal neurons using the liCHi-C method. To complement these data with functional insights, we conducted an RNA-seq analysis of bulk dorsal hippocampus. Using this approach, we characterized age-associated changes in promoter interactions and gene expression. For example, we describe a chromatin loop formation at the *Selenow* promoter, concomitant with an increase in *Selenow* expression with aging, suggesting a neuroprotective role during aging against oxidative stress[62,63] and Alzheimer's disease.[65,66] Moreover, we exposed young and old mice to EE and observed an effect at chromatin interactome and gene expression levels, supporting the notion that external stimuli can modulate these molecular layers in brain.[30]

After characterizing the molecular landscape in the context of aging and EE in hippocampal neurons, we aimed to elucidate the relationship between these two processes. We observed that the overlap in promoter interactions between EE in young and EE in old mice was minimal, approaching what would be expected by chance. This finding demonstrates that the effects of EE differ substantially depending on the age. However, we did observe an association between the promoter interactions affected by aging and by EE in both young and old mice. Remarkably, analyzing the directionality of these changes in promoter interactions, we observed a strong negative correlation between those interactions that were significantly altered by both aging and EE in old mice but a strong positive correlation between interactions altered by both aging and by EE in young mice. A similar pattern was observed at the gene expression level. Therefore, our findings demonstrate that EE produces different effects in young and old mice on the 3D chromatin interactome and gene expression, significantly impacting aging-associated changes but in opposite directions: inducing aging-like changes in young mice while reversing alterations in old mice.

With EE in old individuals, we observed a partial reversion of promoter interactions in the hippocampus associated with EE. This is consistent with previous findings that highlight how EE can reverse alterations associated with aging at the behavioral, physiological, and molecular levels in old mice. At the behavioral level, EE significantly improves spatial memory and restores learning capacity in old animals,[46,74–77] which underscores the

(B) Scatterplot indicating a back-to-back comparison of $\log_2$ fold change of genes ($p < 0.05$, black dots) and DEGs (adj. $p < 0.05$; red dots) for aging and EE in young mice (Pearson's correlation score = 0.938; $p < 2.2e{-}16$). The orange line indicates the regression line (slope and R^2 value are shown), and the gray shade represents the confidence interval.

(C) Scatterplot indicating a back-to-back comparison of $\log_2$ fold change genes ($p < 0.05$, black dots) and DEGs (adj. $p < 0.05$; red dots) for aging and EE in old mice (Pearson's correlation score = −0.598; $p < 2.2e{-}16$). Blue line indicates the regression line (slope and R^2 value are shown), and the gray shade represents the confidence interval.

(D and E) Bar plots reflecting the normalized enrichment score (NES) of GSEA gene sets from the M2 collection (MSigDB). Gene set NESs for aging (old vs. young) and EE in young mice (D) or for aging and EE in old mice (E) are shown (FDR $q < 0.05$). Gene sets were grouped in clusters based on NES signs. Also see Table S6.

(F) *Ndnf* promoter-centered interactions according to liCHi-C data in young, old, and young with environmental enrichment (YEE) conditions. Arcs represent CHiCAGO significant contacts; red arcs highlight those contacts in young mice that were lost in old and YEE mice. Purple shade depicts the gene promoter, and yellow shade depicts a region with significantly altered interactions between the represented conditions (old vs. young; YEE vs. young).

(G) Boxplot indicating the RNA-seq expression measurements (VST normalized data) for the *Ndnf* gene across young, old, and YEE mice. The median scores for each condition are indicated. Boxes represent the interquartile range (IQR), and whiskers extend to the most extreme data points within 1.5 × IQR. Dots denote individual mouse data.

(H) *P2rx5* promoter-centered interactions, according to liCHi-C data in young, old, and old with environmental enrichment (OEE) conditions. Arcs represent CHiCAGO significant contacts; green arcs highlight those contacts that are found only in old mice and not in young or OEE mice. Purple shade depicts the gene promoter and yellow shade depicts a region with significantly altered interactions between represented conditions (old vs. young; OEE vs. old) (see also Table S7). Arrows symbolize gene placement and orientation along the genomic window.

(I) Boxplot indicating the RNA-seq expression measurements for *P2rx5* gene across young, old, and OEE mice. The median scores for each condition are indicated. Boxes represent the IQR, and whiskers extend to the most extreme data points within 1.5 × IQR. Dots denote individual mouse data.

^{ns}adj. $p < 0.05$, *adj. $p < 0.05$, and **adj. $p < 0.01$. Also see Figure S9.

impact of enrichment on the recovery of cognitive functions. Moreover, EE stimulates neurogenesis in old mice, leading to greater neuronal plasticity.[67,78] Finally, age-associated alterations were reversed by EE at different epigenetic modifications in brain.[47,75,79,80] Taken together, our results and these previous studies reinforce the idea that EE not only mitigates cognitive decline but can partially reverse the functional and molecular effects of aging, restoring typical characteristics of younger animals, i.e., promoting brain rejuvenation.[49]

On the other hand, for young mice exposed to EE, we observed an induction of aging-like alterations in the chromatin interactome. Several investigations have been conducted in young mice, describing numerous effects of EE on brain development, for instance, enhancing neurogenesis, synaptic plasticity, spatial learning, and memory, among others.[48,81–83] Also, at the neuron level, EE has been associated with cell survival and proliferation,[84,85] spine formation and maturation,[86] synaptogenesis,[87] and persistence of hippocampal Cajal-Retzius neurons,[88] suggesting that EE could prolong development into adulthood. Moreover, external stimuli, including EE, also foster the acquisition of experiences, learning, and memory consolidation, which could promote or accelerate brain maturation.[89] For instance, external stimuli accelerate the generation and maturation of dentate granule cells on hippocampus,[90] and EE accelerates visual system development.[91] Additionally, EE in young individuals seems to modulate the hippocampus at the epigenetic and chromatin levels, probably associated with a regulation of cognition.[30] All this suggests that EE has a modulation role in neuronal development and hippocampal maturation. Therefore, we can speculate that some of the chromatin interactome alterations that occur in the hippocampus during aging may also be induced by cognitive and physical stimulation, affecting neuron development and promoting maturation of the brain in young individuals. However, further studies are needed to elucidate the effect of EE on epigenetics in young brains.

In summary, we have characterized alterations in the chromatin interactome upon aging in hippocampal neurons, focusing on promoter interactions and their functional implications at the transcription level. Moreover, we reveal an age-dependent effect of an external factor (EE) that may lead to partial neuronal rejuvenation in old mice and potentially promote development and maturation of the hippocampus in young individuals. Further research will shed light on the effects of different external stimuli on young brains and elucidate their reversal potential for aged hippocampi.

Limitations of the study

While we do observe an age-dependent pattern at the 3D chromatin interactome and gene expression levels, this study presented some technical limitations. Our results were achieved using different starting materials for the analysis of the chromatin interactome of NeuN$^+$ hippocampal neurons and of the transcriptome of the whole hippocampus (where over 60% of cells are NeuN$^+$ neurons) due to technical constraints. Future research using recently described techniques such as HiRES,[92] GAGE-seq,[93] or LiMCA,[94] which enable the capture of chromatin architecture and transcription data from the same cells, may facilitate the interpretation of different molecular layers, obtaining a comprehensive characterization of alterations in the hippocampus with different processes.

We also recognize that the modest correlation between promoter interactions and transcription level, which could be dependent on the genomic context, likely highlights the importance of integrating different regulatory layers (chromatin accessibility, transcription factor binding, histone modifications, RNA processing, etc.). Future multiomics and longitudinal approaches will be essential to decipher the complex regulatory mechanism of gene expression.

RESOURCE AVAILABILITY

Lead contact

Requests for further information and resources should be directed to and will be fulfilled by the lead contact, Mario F. Fraga (mffraga@cinn.es).

Materials availability

This study did not generate new unique reagents.

Data and code availability

All data are available in the main text or the supplemental information. Additionally, the raw liCHi-C and RNA-seq data are available in the European Nucleotide Archive (ENA): PRJEB75484 (liCHi-C data) and PRJEB90576 (RNA-seq data). Chromatin state annotations from a previous study[51] are available at Zenodo: https://doi.org/10.5281/zenodo.8372431. Code and processed data underlying this study are publicly available at Zenodo: https://doi.org/10.5281/zenodo.15694108.

ACKNOWLEDGMENTS

We are grateful to the Scientific and Technical Services (STSs) of the University of Oviedo, including the animal facilities of the University of Oviedo, and especially to Ana Cristina Salas Bustamante for her positive contribution to the project. This work has been funded by Instituto de Salud Carlos III (ISCIII) (grants PI21/01067 and PI24/00641 to M.F.F. and A.F.F.) and co-funded by the European Union, the Spanish Association against Cancer (Fundación científica de la AECC) (PRYGN235109FERN to M.F.F.), the Asturias government (PCTI) cofunding 2018–2023/Fondo Europeo de Desarrollo Regional (FEDER) from the European Union (IDI/2021/000077 and IDI/2024/000744 to M.F.F.), Spanish Biomedical Research Network in Rare Diseases (CIBERER) Acciones Cooperativas y Complementarias Intramurales (ACCI20-34-U766 to M.F.F.), Health Research Institute of the Principality of Asturias (ISPA) and the Asociación Galbán (2021-052-INTRAMUR GALBAN-GOURR to R.G.U. and 2023-165-GALBAN-TEVAJ to J.R.T.), ISPA-Jannsen (2021-048-INTRAMURAL NOV-TEVAR to J.R.T.), the eprObes project funded by the European Union through the Horizon Europe Framework Programme (GA 101080219), and ERA-NET TRANSCAN-3 initiative (JTC 2023) (AC24/00163 to M.F.F.). The laboratory of B.M.J. is supported by FEDER/Spanish Ministry of Science and Innovation (PID2021-125277OB-I00). J.G.-V. is supported by the Spanish Ministry of Universities (FPU20/04659). R.G.U. is supported by the Centro de Investigación Biomédica en Red (CIBER). J.R.T. is supported by a Ramon y Cajal contract from the Spanish Ministry of Science and Innovation (RYC2021-031799-I). R.F.P. (BP17-114) and P.S.-O. (BP17-165) are supported by the Severo Ochoa program. A.R. is supported by the Spanish National Research Council (CSIC) (SOLAUT_00038505 SGL2103040) and eprObes project (GA 101080219). J.M.K. is supported by an ARISTOS fellowship (ARISTOS has received funding from the European Union's Horizon Europe Research and Innovation Programme under the Marie Sklodowska-Curie grant agreement no. 101081334). L.T.-D. is supported by the FPI Fellowship (PRE2019-088005). L.R. is supported by an AGAUR FI fellowship (2019FI-B00017). B.M.J. is supported by the Instituto de Salud Carlos III (ISCIII) (CP22/00127). We also acknowledge support from the Institute of Oncology of Asturias (IUOPA, supported by Obra Social Cajastur Liberbank, Spain), the Health Research

Institute of Asturias (ISPA-FINBA), and Consorcio Centro de Investigación Biomédica en Red de Enfermedades Raras (CIBERER-ISCIII).

AUTHOR CONTRIBUTIONS

J.G.-V., R.G.U., A.F.F., and M.F.F. conceived, coordinated, and supervised the study. J.G.-V. and R.G.U. designed all aspects of research, performed environmental enrichment experiments, processed samples, analyzed and interpreted the data, and wrote the manuscript. A.F.F., M.F.F., J.M.K., and J.L.T. participated in drafting the manuscript. A.P., P.S.-O., A.R., and M.R.-S. performed environmental enrichment experiments. J.R.T., R.F.P., and C.A.-D. performed computational analyses and interpreted the data. L.T.-D., L.R., and B.M.J. performed liCHi-C experiments. All authors revised, read, and approved the final manuscript.

DECLARATION OF INTERESTS

The authors declare no competing interests.

STAR★METHODS

Detailed methods are provided in the online version of this paper and include the following:

- KEY RESOURCES TABLE
- EXPERIMENTAL MODEL AND STUDY PARTICIPANT DETAILS
  - Mouse model
  - Environmental enrichment
- METHOD DETAILS
  - Nuclei extraction and fixation
  - Neuronal nuclei purification
  - Low input Promoter Capture Hi-C procedure
  - LiCHi-C processing
  - LiCHi-C interaction calling
  - Histone and chromatin state enrichment
  - Differential analysis of interactions
  - Differential analysis of histone marks
  - Gene ontologies enrichment analysis
  - RNA extraction and library preparation
  - RNA-seq processing
  - Differential gene expression analysis
  - Principal component analysis
  - Gene set enrichment analysis
  - Data visualization
- QUANTIFICATION AND STATISTICAL ANALYSIS
  - Statistical analysis

SUPPLEMENTAL INFORMATION

Supplemental information can be found online at https://doi.org/10.1016/j.celrep.2025.116182.

Received: February 7, 2025
Revised: June 19, 2025
Accepted: July 31, 2025
Published: August 22, 2025

REFERENCES

1. Wagner, K.-H., Cameron-Smith, D., Wessner, B., and Franzke, B. (2016). Biomarkers of Aging: From Function to Molecular Biology. Nutrients *8*, 338. https://doi.org/10.3390/nu8060338.
2. Da Silva, P.F.L., and Schumacher, B. (2021). Principles of the Molecular and Cellular Mechanisms of Aging. J. Invest. Dermatol. *141*, 951–960. https://doi.org/10.1016/j.jid.2020.11.018.
3. Pal, S., and Tyler, J.K. (2016). Epigenetics and aging. Sci. Adv. *2*, e1600584. https://doi.org/10.1126/sciadv.1600584.
4. Sen, P., Shah, P.P., Nativio, R., and Berger, S.L. (2016). Epigenetic Mechanisms of Longevity and Aging. Cell *166*, 822–839. https://doi.org/10.1016/j.cell.2016.07.050.
5. Saul, D., and Kosinsky, R.L. (2021). Epigenetics of Aging and Aging-Associated Diseases. Int. J. Mol. Sci. *22*, 401. https://doi.org/10.3390/ijms22010401.
6. Bettio, L.E.B., Rajendran, L., and Gil-Mohapel, J. (2017). The effects of aging in the hippocampus and cognitive decline. Neurosci. Biobehav. Rev. *79*, 66–86. https://doi.org/10.1016/j.neubiorev.2017.04.030.
7. Kheirbek, M.A., and Hen, R. (2011). Dorsal vs Ventral Hippocampal Neurogenesis: Implications for Cognition and Mood. Neuropsychopharmacology *36*, 373–374. https://doi.org/10.1038/npp.2010.148.
8. Akbarian, S., Beeri, M.S., and Haroutunian, V. (2013). Epigenetic Determinants of Healthy and Diseased Brain Aging and Cognition. JAMA Neurol. *70*, 711–718. https://doi.org/10.1001/jamaneurol.2013.1459.
9. Lardenoije, R., Iatrou, A., Kenis, G., Kompotis, K., Steinbusch, H.W.M., Mastroeni, D., Coleman, P., Lemere, C.A., Hof, P.R., Van Den Hove, D.L.A., and Rutten, B.P.F. (2015). The epigenetics of aging and neurodegeneration. Prog. Neurobiol. *131*, 21–64. https://doi.org/10.1016/j.pneurobio.2015.05.002.
10. Feil, R., and Fraga, M.F. (2012). Epigenetics and the environment: emerging patterns and implications. Nat. Rev. Genet. *13*, 97–109. https://doi.org/10.1038/nrg3142.
11. Cavalli, G., and Heard, E. (2019). Advances in epigenetics link genetics to the environment and disease. Nature *571*, 489–499. https://doi.org/10.1038/s41586-019-1411-0.
12. Urdinguio, R.G., Tejedor, J.R., Fernández-Sanjurjo, M., Pérez, R.F., Peñarroya, A., Ferrero, C., Codina-Martínez, H., Díez-Planelles, C., Pinto-Hernández, P., Castilla-Silgado, J., et al. (2021). Physical exercise shapes the mouse brain epigenome. Mol. Metab. *54*, 101398. https://doi.org/10.1016/j.molmet.2021.101398.
13. Day, J.J., and Sweatt, J.D. (2011). Epigenetic Mechanisms in Cognition. Neuron *70*, 813–829. https://doi.org/10.1016/j.neuron.2011.05.019.
14. Stefanelli, G., Walters, B.J., Ramzan, F., Narkaj, K., Tao, C., and Zovkic, I.B. (2018). Epigenetic Mechanisms of Learning and Memory. In Molecular-Genetic and Statistical Techniques for Behavioral and Neural Research (Elsevier), pp. 345–382. https://doi.org/10.1016/B978-0-12-804078-2.00015-5.
15. Covic, M., Karaca, E., and Lie, D.C. (2010). Epigenetic regulation of neurogenesis in the adult hippocampus. Heredity *105*, 122–134. https://doi.org/10.1038/hdy.2010.27.
16. Yao, B., Christian, K.M., He, C., Jin, P., Ming, G.L., and Song, H. (2016). Epigenetic mechanisms in neurogenesis. Nat. Rev. Neurosci. *17*, 537–549. https://doi.org/10.1038/nrn.2016.70.
17. Levenson, J.M., Roth, T.L., Lubin, F.D., Miller, C.A., Huang, I.-C., Desai, P., Malone, L.M., and Sweatt, J.D. (2006). Evidence That DNA (Cytosine-5) Methyltransferase Regulates Synaptic Plasticity in the Hippocampus. J. Biol. Chem. *281*, 15763–15773. https://doi.org/10.1074/jbc.M511767200.
18. Berson, A., Nativio, R., Berger, S.L., and Bonini, N.M. (2018). Epigenetic Regulation in Neurodegenerative Diseases. Trends Neurosci. *41*, 587–598. https://doi.org/10.1016/j.tins.2018.05.005.
19. Zannas, A.S., and Chrousos, G.P. (2017). Epigenetic programming by stress and glucocorticoids along the human lifespan. Mol. Psychiatry *22*, 640–646. https://doi.org/10.1038/mp.2017.35.
20. Mohanta, T.K., Mishra, A.K., and Al-Harrasi, A. (2021). The 3D Genome: From Structure to Function. Int. J. Mol. Sci. *22*, 11585. https://doi.org/10.3390/ijms222111585.
21. Krijger, P.H.L., and De Laat, W. (2016). Regulation of disease-associated gene expression in the 3D genome. Nat. Rev. Mol. Cell Biol. *17*, 771–782. https://doi.org/10.1038/nrm.2016.138.

22. Stadhouders, R., Filion, G.J., and Graf, T. (2019). Transcription factors and 3D genome conformation in cell-fate decisions. Nature *569*, 345–354. https://doi.org/10.1038/s41586-019-1182-7.

23. Xu, H., Zhang, S., Yi, X., Plewczynski, D., and Li, M.J. (2020). Exploring 3D chromatin contacts in gene regulation: The evolution of approaches for the identification of functional enhancer-promoter interaction. Comput. Struct. Biotechnol. J. *18*, 558–570. https://doi.org/10.1016/j.csbj.2020.02.013.

24. Van Mierlo, G., Pushkarev, O., Kribelbauer, J.F., and Deplancke, B. (2023). Chromatin modules and their implication in genomic organization and gene regulation. Trends Genet. *39*, 140–153. https://doi.org/10.1016/j.tig.2022.11.003.

25. Zuin, J., Roth, G., Zhan, Y., Cramard, J., Redolfi, J., Piskadlo, E., Mach, P., Kryzhanovska, M., Tihanyi, G., Kohler, H., et al. (2022). Nonlinear control of transcription through enhancer–promoter interactions. Nature *604*, 571–577. https://doi.org/10.1038/s41586-022-04570-y.

26. Schoenfelder, S., and Fraser, P. (2019). Long-range enhancer–promoter contacts in gene expression control. Nat. Rev. Genet. *20*, 437–455. https://doi.org/10.1038/s41576-019-0128-0.

27. Lieberman-Aiden, E., Van Berkum, N.L., Williams, L., Imakaev, M., Ragoczy, T., Telling, A., Amit, I., Lajoie, B.R., Sabo, P.J., Dorschner, M. O., et al. (2009). Comprehensive Mapping of Long-Range Interactions Reveals Folding Principles of the Human Genome. Science *326*, 289–293. https://doi.org/10.1126/science.1181369.

28. Fraser, J., Williamson, I., Bickmore, W.A., and Dostie, J. (2015). An Overview of Genome Organization and How We Got There: from FISH to Hi-C. Microbiol. Mol. Biol. Rev. *79*, 347–372. https://doi.org/10.1128/MMBR.00006-15.

29. Fernandez-Albert, J., Lipinski, M., Lopez-Cascales, M.T., Rowley, M.J., Martin-Gonzalez, A.M., Del Blanco, B., Corces, V.G., and Barco, A. (2019). Immediate and deferred epigenomic signatures of in vivo neuronal activation in mouse hippocampus. Nat. Neurosci. *22*, 1718–1730. https://doi.org/10.1038/s41593-019-0476-2.

30. Espeso-Gil, S., Holik, A.Z., Bonnin, S., Jhanwar, S., Chandrasekaran, S., Pique-Regi, R., Albaigès-Ràfols, J., Maher, M., Permanyer, J., Irimia, M., et al. (2021). Environmental Enrichment Induces Epigenomic and Genome Organization Changes Relevant for Cognition. Front. Mol. Neurosci. *14*, 664912. https://doi.org/10.3389/fnmol.2021.664912.

31. Marco, A., Meharena, H.S., Dileep, V., Raju, R.M., Davila-Velderrain, J., Zhang, A.L., Adaikkan, C., Young, J.Z., Gao, F., Kellis, M., and Tsai, L. H. (2020). Mapping the epigenomic and transcriptomic interplay during memory formation and recall in the hippocampal engram ensemble. Nat. Neurosci. *23*, 1606–1617. https://doi.org/10.1038/s41593-020-00717-0.

32. Plaza-Jennings, A., Valada, A., and Akbarian, S. (2022). 3D Genome Plasticity in Normal and Diseased Neurodevelopment. Genes *13*, 1999. https://doi.org/10.3390/genes13111999.

33. Song, M., Pebworth, M.-P., Yang, X., Abnousi, A., Fan, C., Wen, J., Rosen, J.D., Choudhary, M.N.K., Cui, X., Jones, I.R., et al. (2020). Cell-type-specific 3D epigenomes in the developing human cortex. Nature *587*, 644–649. https://doi.org/10.1038/s41586-020-2825-4.

34. Lu, L., Liu, X., Huang, W.-K., Giusti-Rodríguez, P., Cui, J., Zhang, S., Xu, W., Wen, Z., Ma, S., Rosen, J.D., et al. (2020). Robust Hi-C Maps of Enhancer-Promoter Interactions Reveal the Function of Non-coding Genome in Neural Development and Diseases. Mol. Cell *79*, 521–534. e15. https://doi.org/10.1016/j.molcel.2020.06.007.

35. Liu, W., Zhong, W., Chen, J., Huang, B., Hu, M., and Li, Y. (2022). Understanding Regulatory Mechanisms of Brain Function and Disease through 3D Genome Organization. Genes *13*, 586. https://doi.org/10.3390/genes13040586.

36. Li, M., Santpere, G., Imamura Kawasawa, Y., Evgrafov, O.V., Gulden, F. O., Pochareddy, S., Sunkin, S.M., Li, Z., Shin, Y., Zhu, Y., et al. (2018). Integrative functional genomic analysis of human brain development and neuropsychiatric risks. Science *362*, eaat7615. https://doi.org/10.1126/science.aat7615.

37. Tan, L., Shi, J., Moghadami, S., Parasar, B., Wright, C.P., Seo, Y., Vallejo, K., Cobos, I., Duncan, L., Chen, R., and Deisseroth, K. (2023). Lifelong restructuring of 3D genome architecture in cerebellar granule cells. Science *381*, 1112–1119. https://doi.org/10.1126/science.adh3253.

38. Sati, S., and Cavalli, G. (2017). Chromosome conformation capture technologies and their impact in understanding genome function. Chromosoma *126*, 33–44. https://doi.org/10.1007/s00412-016-0593-6.

39. Schoenfelder, S., Javierre, B.-M., Furlan-Magaril, M., Wingett, S.W., and Fraser, P. (2018). Promoter Capture Hi-C: High-resolution, Genome-wide Profiling of Promoter Interactions. J. Vis. Exp. *57320*, 57320. https://doi.org/10.3791/57320.

40. Su, C., Argenziano, M., Lu, S., Pippin, J.A., Pahl, M.C., Leonard, M.E., Cousminer, D.L., Johnson, M.E., Lasconi, C., Wells, A.D., et al. (2021). 3D promoter architecture re-organization during iPSC-derived neuronal cell differentiation implicates target genes for neurodevelopmental disorders. Prog. Neurobiol. *201*, 102000. https://doi.org/10.1016/j.pneurobio.2021.102000.

41. Song, M., Yang, X., Ren, X., Maliskova, L., Li, B., Jones, I.R., Wang, C., Jacob, F., Wu, K., Traglia, M., et al. (2019). Mapping cis-regulatory chromatin contacts in neural cells links neuropsychiatric disorder risk variants to target genes. Nat. Genet. *51*, 1252–1262. https://doi.org/10.1038/s41588-019-0472-1.

42. Javierre, B.M., Burren, O.S., Wilder, S.P., Kreuzhuber, R., Hill, S.M., Sewitz, S., Cairns, J., Wingett, S.W., Várnai, C., Thiecke, M.J., et al. (2016). Lineage-Specific Genome Architecture Links Enhancers and Non-coding Disease Variants to Target Gene Promoters. Cell *167*, 1369–1384. e19. https://doi.org/10.1016/j.cell.2016.09.037.

43. Zeisel, A., Muñoz-Manchado, A.B., Codeluppi, S., Lönnerberg, P., La Manno, G., Juréus, A., Marques, S., Munguba, H., He, L., Betsholtz, C., et al. (2015). Cell types in the mouse cortex and hippocampus revealed by single-cell RNA-seq. Science *347*, 1138–1142. https://doi.org/10.1126/science.aaa1934.

44. Nott, A., Holtman, I.R., Coufal, N.G., Schlachetzki, J.C.M., Yu, M., Hu, R., Han, C.Z., Pena, M., Xiao, J., Wu, Y., et al. (2019). Brain cell type–specific enhancer–promoter interactome maps and disease - risk association. Science *366*, 1134–1139. https://doi.org/10.1126/science.aay0793.

45. Tomás-Daza, L., Rovirosa, L., López-Martí, P., Nieto-Aliseda, A., Serra, F., Planas-Riverola, A., Molina, O., McDonald, R., Ghevaert, C., Cuatrecasas, E., et al. (2023). Low input capture Hi-C (liCHi-C) identifies promoter-enhancer interactions at high-resolution. Nat. Commun. *14*, 268. https://doi.org/10.1038/s41467-023-35911-8.

46. Cortese, G.P., Olin, A., O'Riordan, K., Hullinger, R., and Burger, C. (2018). Environmental enrichment improves hippocampal function in aged rats by enhancing learning and memory, LTP, and mGluR5-Homer1c activity. Neurobiol. Aging *63*, 1–11. https://doi.org/10.1016/j.neurobiolaging.2017.11.004.

47. Zocher, S., Overall, R.W., Lesche, M., Dahl, A., and Kempermann, G. (2021). Environmental enrichment preserves a young DNA methylation landscape in the aged mouse hippocampus. Nat. Commun. *12*, 3892. https://doi.org/10.1038/s41467-021-23993-1.

48. Baroncelli, L., Braschi, C., Spolidoro, M., Begenisic, T., Sale, A., and Maffei, L. (2010). Nurturing brain plasticity: impact of environmental enrichment. Cell Death Differ. *17*, 1092–1103. https://doi.org/10.1038/cdd.2009.193.

49. Zocher, S. (2024). Targeting neuronal epigenomes for brain rejuvenation. EMBO J. *43*, 3312–3326. https://doi.org/10.1038/s44318-024-00148-8.

50. Rubio, F.J., Li, X., Liu, Q.-R., Cimbro, R., and Hope, B.T. (2016). Fluorescence Activated Cell Sorting (FACS) and Gene Expression Analysis of Fos-expressing Neurons from Fresh and Frozen Rat Brain Tissue. J. Vis. Exp. *54358*, 54358. https://doi.org/10.3791/54358.

51. Pérez, R.F., Tezanos, P., Peñarroya, A., González-Ramón, A., Urdinguio, R.G., Gancedo-Verdejo, J., Tejedor, J.R., Santamarina-Ojeda, P., Alba-Linares, J.J., Sainz-Ledo, L., et al. (2024). A multiomic atlas of the aging hippocampus reveals molecular changes in response to environmental enrichment. Nat. Commun. *15*, 5829. https://doi.org/10.1038/s41467-024-49608-z.

52. Wingett, S., Ewels, P., Furlan-Magaril, M., Nagano, T., Schoenfelder, S., Fraser, P., and Andrews, S. (2015). HiCUP: pipeline for mapping and processing Hi-C data. F1000Res. *4*, 1310. https://doi.org/10.12688/f1000research.7334.1.

53. Cairns, J., Freire-Pritchett, P., Wingett, S.W., Várnai, C., Dimond, A., Plagnol, V., Zerbino, D., Schoenfelder, S., Javierre, B.-M., Osborne, C., et al. (2016). CHiCAGO: robust detection of DNA looping interactions in Capture Hi-C data. Genome Biol. *17*, 127. https://doi.org/10.1186/s13059-016-0992-2.

54. Koester, J., Miroshnikova, Y.A., Ghatak, S., Chacón-Martínez, C.A., Morgner, J., Li, X., Atanassov, I., Altmüller, J., Birk, D.E., Koch, M., et al. (2021). Niche stiffening compromises hair follicle stem cell potential during ageing by reducing bivalent promoter accessibility. Nat. Cell Biol. *23*, 771–781. https://doi.org/10.1038/s41556-021-00705-x.

55. Cairns, J., Orchard, W.R., Malysheva, V., and Spivakov, M. (2019). Chicdiff: a computational pipeline for detecting differential chromosomal interactions in Capture Hi-C data. Bioinformatics *35*, 4764–4766. https://doi.org/10.1093/bioinformatics/btz450.

56. Cuestas Torres, D.M., and Cardenas, F.P. (2020). Synaptic plasticity in Alzheimer's disease and healthy aging. Rev. Neurosci. *31*, 245–268. https://doi.org/10.1515/revneuro-2019-0058.

57. Subramanian, A., Tamayo, P., Mootha, V.K., Mukherjee, S., Ebert, B.L., Gillette, M.A., Paulovich, A., Pomeroy, S.L., Golub, T.R., Lander, E.S., and Mesirov, J.P. (2005). Gene set enrichment analysis: A knowledge-based approach for interpreting genome-wide expression profiles. Proc. Natl. Acad. Sci. *102*, 15545–15550. https://doi.org/10.1073/pnas.0506580102.

58. Li, B., Carey, M., and Workman, J.L. (2007). The Role of Chromatin during Transcription. Cell *128*, 707–719. https://doi.org/10.1016/j.cell.2007.01.015.

59. Bernstein, B.E., Mikkelsen, T.S., Xie, X., Kamal, M., Huebert, D.J., Cuff, J., Fry, B., Meissner, A., Wernig, M., Plath, K., et al. (2006). A bivalent chromatin structure marks key developmental genes in embryonic stem cells. Cell *125*, 315–326. https://doi.org/10.1016/j.cell.2006.02.041.

60. Swarnkar, S., Avchalumov, Y., Raveendra, B.L., Grinman, E., and Puthanveettil, S.V. (2018). Kinesin Family of Proteins Kif11 and Kif21B Act as Inhibitory Constraints of Excitatory Synaptic Transmission Through Distinct Mechanisms. Sci. Rep. *8*, 17419. https://doi.org/10.1038/s41598-018-35634-7.

61. Falnikar, A., Tole, S., and Baas, P.W. (2011). Kinesin-5, a mitotic microtubule-associated motor protein, modulates neuronal migration. Mol. Biol. Cell *22*, 1561–1574. https://doi.org/10.1091/mbc.e10-11-0905.

62. Chung, Y.W., Jeong, D., Noh, O.J., Park, Y.H., Kang, S.I., Lee, M.G., Lee, T.-H., Yim, M.B., and Kim, I.Y. (2009). Antioxidative Role of Selenoprotein W in Oxidant-Induced Mouse Embryonic Neuronal Cell Death. Mol. Cells *27*, 609–613. https://doi.org/10.1007/s10059-009-0074-3.

63. Behl, S., Mehta, S., and Pandey, M.K. (2023). The role of selenoproteins in neurodevelopment and neurological function: Implications in autism spectrum disorder. Front. Mol. Neurosci. *16*, 1130922. https://doi.org/10.3389/fnmol.2023.1130922.

64. Situ, J., Huang, X., Zuo, M., Huang, Y., Ren, B., and Liu, Q. (2022). Comparative Proteomic Analysis Reveals the Effect of Selenoprotein W Deficiency on Oligodendrogenesis in Fear Memory. Antioxidants *11*, 999. https://doi.org/10.3390/antiox11050999.

65. Zhang, Z.-H., and Song, G.-L. (2021). Roles of Selenoproteins in Brain Function and the Potential Mechanism of Selenium in Alzheimer's Disease. Front. Neurosci. *15*, 646518. https://doi.org/10.3389/fnins.2021.646518.

66. Chen, H., Liu, S., Li, S., Chen, J., Ni, J., and Liu, Q. (2018). Blocking the Thiol at Cysteine-322 Destabilizes Tau Protein and Prevents Its Oligomer Formation. ACS Chem. Neurosci. *9*, 1560–1565. https://doi.org/10.1021/acschemneuro.8b00003.

67. Speisman, R.B., Kumar, A., Rani, A., Pastoriza, J.M., Severance, J.E., Foster, T.C., and Ormerod, B.K. (2013). Environmental enrichment restores neurogenesis and rapid acquisition in aged rats. Neurobiol. Aging *34*, 263–274. https://doi.org/10.1016/j.neurobiolaging.2012.05.023.

68. Martínez, G., Vidal, R.L., Mardones, P., Serrano, F.G., Ardiles, A.O., Wirth, C., Valdés, P., Thielen, P., Schneider, B.L., Kerr, B., et al. (2016). Regulation of Memory Formation by the Transcription Factor XBP1. Cell Rep. *14*, 1382–1394. https://doi.org/10.1016/j.celrep.2016.01.028.

69. O'Connor, T.P., Cockburn, K., Wang, W., Tapia, L., Currie, E., and Bamji, S.X. (2009). Semaphorin 5B mediates synapse elimination in hippocampal neurons. Neural Dev. *4*, 18. https://doi.org/10.1186/1749-8104-4-18.

70. Lein, E.S., Hawrylycz, M.J., Ao, N., Ayres, M., Bensinger, A., Bernard, A., Boe, A.F., Boguski, M.S., Brockway, K.S., Byrnes, E.J., et al. (2007). Genome-wide atlas of gene expression in the adult mouse brain. Nature *445*, 168–176. https://doi.org/10.1038/nature05453.

71. Kuang, X.-L., Zhao, X.-M., Xu, H.-F., Shi, Y.-Y., Deng, J.-B., and Sun, G.-T. (2010). Spatio-temporal expression of a novel neuron-derived neurotrophic factor (NDNF) in mouse brains during development. BMC Neurosci. *11*, 137. https://doi.org/10.1186/1471-2202-11-137.

72. Guo, W., Xu, X., Gao, X., Burnstock, G., He, C., and Xiang, Z. (2008). Expression of P2X5 receptors in the mouse CNS. Neuroscience *156*, 673–692. https://doi.org/10.1016/j.neuroscience.2008.07.062.

73. Guo, W., Zhang, Z., Liu, X., Burnstock, G., Xiang, Z., and He, C. (2013). Developmental expression of P2X5 receptors in the mouse prenatal central and peripheral nervous systems. Purinergic Signal. *9*, 239–248. https://doi.org/10.1007/s11302-012-9346-z.

74. Freret, T., Billard, J.-M., Schumann-Bard, P., Dutar, P., Dauphin, F., Boulouard, M., and Bouet, V. (2012). Rescue of cognitive aging by long-lasting environmental enrichment exposure initiated before median lifespan. Neurobiol. Aging *33*, 1005.e1–1005.e10. https://doi.org/10.1016/j.neurobiolaging.2011.09.028.

75. Fischer, A., Sananbenesi, F., Wang, X., Dobbin, M., and Tsai, L.-H. (2007). Recovery of learning and memory is associated with chromatin remodelling. Nature *447*, 178–182. https://doi.org/10.1038/nature05772.

76. Frick, K.M., and Fernandez, S.M. (2003). Enrichment enhances spatial memory and increases synaptophysin levels in aged female mice. Neurobiol. Aging *24*, 615–626. https://doi.org/10.1016/S0197-4580(02)00138-0.

77. Bennett, J.C., McRae, P.A., Levy, L.J., and Frick, K.M. (2006). Long-term continuous, but not daily, environmental enrichment reduces spatial memory decline in aged male mice. Neurobiol. Learn. Mem. *85*, 139–152. https://doi.org/10.1016/j.nlm.2005.09.003.

78. Kempermann, G., Kuhn, H.G., and Gage, F.H. (1998). Experience-Induced Neurogenesis in the Senescent Dentate Gyrus. J. Neurosci. *18*, 3206–3212. https://doi.org/10.1523/JNEUROSCI.18-09-03206.1998.

79. Morse, S.J., Butler, A.A., Davis, R.L., Soller, I.J., and Lubin, F.D. (2015). Environmental Enrichment Reverses Histone Methylation Changes in the Aged Hippocampus and Restores Age-Related Memory Deficits. Biology *4*, 298–313. https://doi.org/10.3390/biology4020298.

80. Irier, H., Street, R.C., Dave, R., Lin, L., Cai, C., Davis, T.H., Yao, B., Cheng, Y., and Jin, P. (2014). Environmental enrichment modulates 5-hydroxymethylcytosine dynamics in hippocampus. Genomics *104*, 376–382. https://doi.org/10.1016/j.ygeno.2014.08.019.

81. Sale, A., Berardi, N., and Maffei, L. (2009). Enrich the environment to empower the brain. Trends Neurosci. *32*, 233–239. https://doi.org/10.1016/j.tins.2008.12.004.

82. Sale, A. (2018). A Systematic Look at Environmental Modulation and Its Impact in Brain Development. Trends Neurosci. *41*, 4–17. https://doi.org/10.1016/j.tins.2017.10.004.

83. Nithianantharajah, J., and Hannan, A.J. (2006). Enriched environments, experience-dependent plasticity and disorders of the nervous system. Nat. Rev. Neurosci. *7*, 697–709. https://doi.org/10.1038/nrn1970.

84. Kempermann, G., Kuhn, H.G., and Gage, F.H. (1997). More hippocampal neurons in adult mice living in an enriched environment. Nature *386*, 493–495. https://doi.org/10.1038/386493a0.

85. Kempermann, G., and Gage, F.H. (1999). Experience-dependent regulation of adult hippocampal neurogenesis: Effects of long-term stimulation and stimulus withdrawal. Hippocampus *9*, 321–332. https://doi.org/10.1002/(SICI)1098-1063(1999)9:3<321::AID-HIPO11>3.0.CO;2-C.

86. Zhao, C., Jou, J., Wolff, L.J., Sun, H., and Gage, F.H. (2014). Spine morphogenesis in newborn granule cells is differentially regulated in the outer and middle molecular layers. J. Comp. Neurol. *522*, 2756–2766. https://doi.org/10.1002/cne.23581.

87. Nithianantharajah, J., Levis, H., and Murphy, M. (2004). Environmental enrichment results in cortical and subcortical changes in levels of synaptophysin and PSD-95 proteins. Neurobiol. Learn. Mem. *81*, 200–210. https://doi.org/10.1016/j.nlm.2004.02.002.

88. Anstötz, M., Lee, S.K., Neblett, T.I., Rune, G.M., and Maccaferri, G. (2018). Experience-Dependent Regulation of Cajal–Retzius Cell Networks in the Developing and Adult Mouse Hippocampus. Cereb. Cortex *28*, 672–687. https://doi.org/10.1093/cercor/bhx153.

89. Bath, K., Manzano-Nieves, G., and Goodwill, H. (2016). Early life stress accelerates behavioral and neural maturation of the hippocampus in male mice. Horm. Behav. *82*, 64–71. https://doi.org/10.1016/j.yhbeh.2016.04.010.

90. Liu, N., He, S., and Yu, X. (2012). Early Natural Stimulation through Environmental Enrichment Accelerates Neuronal Development in the Mouse Dentate Gyrus. PLoS One *7*, e30803. https://doi.org/10.1371/journal.pone.0030803.

91. Cancedda, L., Putignano, E., Sale, A., Viegi, A., Berardi, N., and Maffei, L. (2004). Acceleration of Visual System Development by Environmental Enrichment. J. Neurosci. *24*, 4840–4848. https://doi.org/10.1523/JNEUROSCI.0845-04.2004.

92. Liu, Z., Chen, Y., Xia, Q., Liu, M., Xu, H., Chi, Y., Deng, Y., and Xing, D. (2023). Linking genome structures to functions by simultaneous single-cell Hi-C and RNA-seq. Science *380*, 1070–1076. https://doi.org/10.1126/science.adg3797.

93. Zhou, T., Zhang, R., Jia, D., Doty, R.T., Munday, A.D., Gao, D., Xin, L., Abkowitz, J.L., Duan, Z., and Ma, J. (2024). GAGE-seq concurrently profiles multiscale 3D genome organization and gene expression in single cells. Nat. Genet. *56*, 1701–1711. https://doi.org/10.1038/s41588-024-01745-3.

94. Wu, H., Zhang, J., Jian, F., Chen, J.P., Zheng, Y., Tan, L., and Sunney Xie, X. (2024). Simultaneous single-cell three-dimensional genome and gene expression profiling uncovers dynamic enhancer connectivity underlying olfactory receptor choice. Nat. Methods *21*, 974–982. https://doi.org/10.1038/s41592-024-02239-0.

95. Geifman, N., Monsonego, A., and Rubin, E. (2010). The Neural/Immune Gene Ontology: clipping the Gene Ontology for neurological and immunological systems. BMC Bioinf. *11*, 458. https://doi.org/10.1186/1471-2105-11-458.

96. Koopmans, F., Van Nierop, P., Andres-Alonso, M., Byrnes, A., Cijsouw, T., Coba, M.P., Cornelisse, L.N., Farrell, R.J., Goldschmidt, H.L., Howrigan, D.P., et al. (2019). SynGO: An Evidence-Based, Expert-Curated Knowledge Base for the Synapse. Neuron *103*, 217–234.e4. https://doi.org/10.1016/j.neuron.2019.05.002.

97. Castanza, A.S., Recla, J.M., Eby, D., Thorvaldsdóttir, H., Bult, C.J., and Mesirov, J.P. (2023). Extending support for mouse data in the Molecular Signatures Database (MSigDB). Nat. Methods *20*, 1619–1620. https://doi.org/10.1038/s41592-023-02014-7.

98. Langmead, B., and Salzberg, S.L. (2012). Fast gapped-read alignment with Bowtie 2. Nat. Methods *9*, 357–359. https://doi.org/10.1038/nmeth.1923.

99. Freire-Pritchett, P., Ray-Jones, H., Della Rosa, M., Eijsbouts, C.Q., Orchard, W.R., Wingett, S.W., Wallace, C., Cairns, J., Spivakov, M., and Malysheva, V. (2021). Detecting chromosomal interactions in Capture Hi-C data with CHiCAGO and companion tools. Nat. Protoc. *16*, 4144–4176. https://doi.org/10.1038/s41596-021-00567-5.

100. Kolde, R. (2010). pheatmap: Pretty Heatmaps. R Package Version 1, 726. https://doi.org/10.32614/CRAN.package.pheatmap.

101. Ross-Innes, C.S., Stark, R., Teschendorff, A.E., Holmes, K.A., Ali, H.R., Dunning, M.J., Brown, G.D., Gojis, O., Ellis, I.O., Green, A.R., et al. (2012). Differential oestrogen receptor binding is associated with clinical outcome in breast cancer. Nature *481*, 389–393. https://doi.org/10.1038/nature10730.

102. Lawrence, M., Huber, W., Pagès, H., Aboyoun, P., Carlson, M., Gentleman, R., Morgan, M.T., and Carey, V.J. (2013). Software for Computing and Annotating Genomic Ranges. PLoS Comput. Biol. *9*, e1003118. https://doi.org/10.1371/journal.pcbi.1003118.

103. Wu, T., Hu, E., Xu, S., Chen, M., Guo, P., Dai, Z., Feng, T., Zhou, L., Tang, W., Zhan, L., et al. (2021). clusterProfiler 4.0: A universal enrichment tool for interpreting omics data. Innovation *2*, 100141. https://doi.org/10.1016/j.xinn.2021.100141.

104. Sayols, S. (2023). rrvgo: a Bioconductor package to reduce and visualize Gene Ontology terms. microPublication Biology. https://doi.org/10.17912/micropub.biology.000811.

105. Chen, S., Zhou, Y., Chen, Y., and Gu, J. (2018). fastp: an ultra-fast all-in-one FASTQ preprocessor. Bioinformatics *34*, i884–i890. https://doi.org/10.1093/bioinformatics/bty560.

106. Patro, R., Duggal, G., Love, M.I., Irizarry, R.A., and Kingsford, C. (2017). Salmon provides fast and bias-aware quantification of transcript expression. Nat. Methods *14*, 417–419. https://doi.org/10.1038/nmeth.4197.

107. Soneson, C., Love, M.I., and Robinson, M.D. (2015). Differential analyses for RNA-seq: transcript-level estimates improve gene-level inferences. F1000Res. *4*, 1521. https://doi.org/10.12688/f1000research.7563.2.

108. Durinck, S., Moreau, Y., Kasprzyk, A., Davis, S., De Moor, B., Brazma, A., and Huber, W. (2005). BioMart and Bioconductor: a powerful link between biological databases and microarray data analysis. Bioinformatics *21*, 3439–3440. https://doi.org/10.1093/bioinformatics/bti525.

109. Robinson, M.D., McCarthy, D.J., and Smyth, G.K. (2010). edgeR : a Bioconductor package for differential expression analysis of digital gene expression data. Bioinformatics *26*, 139–140. https://doi.org/10.1093/bioinformatics/btp616.

110. Love, M.I., Huber, W., and Anders, S. (2014). Moderated estimation of fold change and dispersion for RNA-seq data with DESeq2. Genome Biol. *15*, 550. https://doi.org/10.1186/s13059-014-0550-8.

111. Murdoch, D., and Adler, D. (2004). rgl: 3D Visualization Using OpenGL. R Found. https://doi.org/10.32614/cran.package.rgl.

112. Wickham, H. (2009). ggplot2: Elegant Graphics for Data Analysis (Springer). https://doi.org/10.1007/978-0-387-98141-3.

113. Larsson, J., and Gustafsson, P. (2018). A case study in fitting area-proportional euler diagrams with ellipses using eulerr. In: Proceedings of the International Workshop on Set Visualization and Reasoning, Y. Sato and Z. Shams, eds., CEUR Workshop Proceedings, p. 84–91.

114. Li, D., Purushotham, D., Harrison, J.K., Hsu, S., Zhuo, X., Fan, C., Liu, S., Xu, V., Chen, S., Xu, J., et al. (2022). WashU Epigenome Browser update 2022. Nucleic Acids Res. *50*, W774–W781. https://doi.org/10.1093/nar/gkac238.

115. Rovirosa, L., Tomás-Daza, L., Urmeneta, B., Valencia, A., and Javierre, B.M. (2023). An Integrated Workflow to Study the Promoter-Centric Spatio-Temporal Genome Architecture in Scarce Cell Populations. J. Vis. Exp. *65316*. https://doi.org/10.3791/65316.

STAR★METHODS

KEY RESOURCES TABLE

REAGENT or RESOURCE	SOURCE	IDENTIFIER
Antibodies		
Mouse monoclonal Alexa Fluor®488-conjugated anti-NeuN (clone A60)	Millipore	Cat#MAB377X; RRID:AB_2149209
Chemicals, peptides, and recombinant proteins		
Triton X-100	Sigma-Aldrich	Cat#T8787; CAS: 9036-19-5
Paraformaldehyde 16% Solution (methanol-free)	Agar Scientifics	Cat#R1026; CAS: 50-00-0
7-AAD staining solution	Biolegend	Cat#420404
HindIII enzyme	New England Biolabs	Cat#R0104T
Biotin-14-dATP	Invitrogen	Cat#19524-016
Klenow polymerase	New England Biolabs	Cat#M0210L
T4 DNA Ligase	Invitrogen	Cat#15224-025
Proteinase K	Roche	Cat#03115879001
Phenol:chloroform:isoamyl alcohol 25:24:1	Sigma-Aldrich	Cat#P3803
Dynabeads MyOne streptavidin C1 paramagnetic beads	Thermo Fisher	Cat#65001
SPRI beads	CleanNA	Cat#CNGS-0050
Critical commercial assays		
DNA D1000 ScreenTape Analysis	Agilent	Cat#5067-5582
RNeasy Mini Kit	Qiagen	Cat#74104
RNase-Free DNase Set	Qiagen	Cat#79254
Qubit RNA HS Assay kit	Thermo Fisher Scientific	Cat#Q32852
NEBNext Ultra II RNA Library Prep Kit	New England Biolabs	Cat#E7770
Deposited data		
liCHi-C sequencing data	This paper	European Nucleotide Archive (ENA): PRJEB75484.
RNA sequencing data	This paper	ENA: PRJEB90576
All code underlying this study	This paper	Zenodo: https://doi.org/10.5281/zenodo.15694108
Chromatin state annotations from ChIP-seq datasets for hippocampus tissue	Perez et al. [51]	Zenodo: https://doi.org/10.5281/zenodo.8372431
Neural-Immune Gene Ontology (NIGO) subset	Geifman et al. [95]	https://scicrunch.org/resolver/SCR_004120; RRID:SCR_004120
Synaptic Gene Ontologies (SynGO) subset	Koopmans et al.[96]	https://syngoportal.org
M2 (curated gene sets) and M5 (ontology gene sets) collections, from the mouse MSigDB v2023.1 (Molecular signatures database)	Castanza et al.[97]	https://www.gsea-msigdb.org/gsea/msigdb
LEIN markets dataset	Lein et al.[70]	https://www.gsea-msigdb.org/gsea/msigdb/mouse/genesets.jsp?collection=CGP
Experimental models: Organisms/strains		
Mouse: C57BL/6JRj (aged)	Janvier Labs	RRID:IMSR_RJ:AGED-C57BL-6JRJ
Oligonucleotides		
Primer for liCHi-C 3C quality control: Calr1: TCATGAGTTCCCCACATCTTTG	Schoenfelder et al.[39]	N/A

(*Continued on next page*)

Continued

REAGENT or RESOURCE	SOURCE	IDENTIFIER
Primer for liCHi-C 3C quality control: Calr3: CTGTGGGCACCAGATGTGTAAAT	Schoenfelder et al.[39]	N/A
Primer for liCHi-C 3C quality control: Hist1h2ae:GGGTAATGGTG TCACTAACTGG	Schoenfelder et al.[39]	N/A
Primer for liCHi-C 3C quality control: Hist1h3e: GGGTTTGATGAGTTGGTGAAG	Schoenfelder et al.[39]	N/A
Primer for liCHi-C 3C quality control: Hist1h4i: TTGGGCCAAAGCCTATATGA	Schoenfelder et al.[39]	N/A
PE adapter used for liCHi-C library construction: PE1 Adapter: 5′ P-GATCGGAAGAGCGGTTCAGCAG GAATGCCGAG 3’	Schoenfelder et al.[39]	N/A
PE adapters used for liCHi-C library construction: PE2 Adapter: 5′ ACACTCTTTCCCTACACGACGCTC TTCCGATC*T 3’	Schoenfelder et al.[39]	N/A
PE primer used for liCHi-C library construction: PE PCR Primer 1: 5’ AATGATACGGCGACCACCGAGA TCTACACTCTTTCCCTACACGAC GCTCTTCCGATCT 3’	Schoenfelder et al.[39]	N/A
PE primer used for liCHi-C library construction: PE PCR Primer 2: 5’CAAGCAGAAGACGGCATACGAG ATCGGTCTCGGCATTCCTGCTGAA CCGCTCTTCCGATCT 3’	Schoenfelder et al.[39]	N/A
Software and algorithms		
Summit software (v5.2.0.7477)	Beckman Coulter	N/A
HiCUP (v0.8.3)	Wingett et al.[52]	www.bioinformatics.babraham.ac.uk/projects/hicup
Bowtie2 (v2.4.1)	Langmead and Salzberg[98]	http://bowtie-bio.sourceforge.net/bowtie2/index.shtml
CHiCAGO (v1.18.0)	Cairns et al.2016[53]; Freire-Pritchett et al.[99]	https://bioconductor.org/packages/release/bioc/html/Chicago.html
pheatmap (v1.0.12)	Kolde[100]	https://github.com/raivokolde/pheatmap
Chicdiff (v0.6)	Cairns et al.[55]	https://github.com/RegulatoryGenomicsGroup/chicdiff
DiffBind (v3.0.15)	Ross-Innes et al.[101]	http://bioconductor.org/packages/release/bioc/html/DiffBind.html
GenomicRanges (v1.54.1)	Lawrence et al.[102]	https://www.bioconductor.org/packages/release/bioc/html/GenomicRanges.html
ClusterProfiler (v4.10.0)	Wu et al.[103]	https://bioconductor.org/packages/release/bioc/html/clusterProfiler.html
rrvgo (v1.14.1)	Sayols[104]	https://www.bioconductor.org/packages/release/bioc/html/rrvgo.html
fastp (v0.20.1)	Chen et al.[105]	https://github.com/OpenGene/fastp
Salmon (v1.5.0)	Patro et al.[106]	https://github.com/COMBINE-lab/salmon
tximport (v1.14.2)	Soneson et al.[107]	http://bioconductor.org/packages/tximport
biomaRt (v2.42.0)	Durinck et al.[108]	https://www.bioconductor.org/packages/release/bioc/html/biomaRt.html
edgeR (v3.28.1)	Robinson et al.[109]	https://bioconductor.org/packages/release/bioc/html/edgeR.html
DESeq2 (v1.26.0)	Love et al.[110]	http://www.bioconductor.org/packages/release/bioc/html/DESeq2.html

(*Continued on next page*)

Continued

REAGENT or RESOURCE	SOURCE	IDENTIFIER
rgl (v1.2.1)	Murdoch and Adler[111]	https://dmurdoch.github.io/rgl/ or https://github.com/dmurdoch/rgl
Gene Set Enrichment Analysis (GSEA) (v4.3.2)	Subramanian et al.[57]	https://www.gsea-msigdb.org/gsea/index.jsp
ggplot2 (v3.4.2)	Wickham[112]	https://ggplot2.tidyverse.org/
eulerr (v7.0.2)	Larsson and Gustafsson[113]	https://github.com/jolars/eulerr
WashU Epigenome Browser (v54.0.3)	Li et al.[114]	https://epigenomegateway.wustl.edu/browser/
Other		
Eurostandard Type IV (large) PVC cages	Biosis	Cat#1354G
Eurostandard Type II L (standard-size) PVC cages	Biosis	Cat#1284L
5 mL Round Bottom Tube with 35 μm Nylon Mesh Snap Cap	Falcon	Cat#352235
MoFlo XDP High-Speed Cell Sorter	Beckman Coulter	Cat#ML99030
DNA LoBind 1.5-ml tubes	Eppendorf	Cat#022431021
Qubit 3.0 Fluorometer	Invitrogen	Cat#Q33216; RRID:SCR_020311
M220 Focused-ultrasonicator	Covaris	RRID:SCR_027073
2200 TapeStation System	Agilent	Cat#G2964AA; RRID:SCR_014994
5300 Fragment Analyzer System	Agilent	Cat#M5311AA; RRID:SCR_019411
Illumina NovaSeq 6000 Sequencing System	Illumina	RRID:SCR_016387

EXPERIMENTAL MODEL AND STUDY PARTICIPANT DETAILS

Mouse model

A total of 60 male C57Bl/6JRj mice (*Mus musculus*), 9 weeks old (30 young mice) and 17 months old (30 old mice), were supplied by Janvier Labs. Mice from each age group were randomly assigned to different experimental groups: 15 to control conditions and 15 exposed to Environmental Enrichment for 2 months. Upon arrival at the Animal Facilities of the University of Oviedo, 5 or 6 animals were housed per cage, and they were acclimated for 2 weeks. Mice were maintained under standard conditions, including 12-hours light/dark cycles, controlled temperature (20-22°C), and *ad libitum* access to food and water, in accordance with the European Union Directive 2010/63/EU. The animals were euthanized by cervical dislocation, and the dorsal hippocampi were isolated from the mouse brains. All procedures were performed in accordance with the Spanish Guidelines (Real Decreto 53/2013) based on the European Union Directive 2010/63/EU for animal research, and were approved by The Research Ethics Committee of the University of Oviedo (PROAE 08/2021).

Environmental enrichment

Young and old mice exposed to environmental enrichment were housed in large PVC cages (Eurostandard Type IV, Biosis, Cat#1354G, 598x380x250 mm) with tunnels, swings, wheels, ramps, houses, and different toys and objects of different shapes, sizes, and textures, randomly distributed throughout the cage. These objects were exchanged between cages every 2-3 days to modify the environmental stimuli and expose the animals to different mice odours. Also, bedding materials were changed every 1-2 weeks. Animals of control group were housed in the same room in standard-size cages (Eurostandard Type II L, Biosis, Cat#1284L, 365x207x140 mm) without access to the objects and toys.

METHOD DETAILS

Nuclei extraction and fixation

Hippocampi were homogenised with a syringe in cold NEB (Nuclei Extraction Buffer: 0.32 M sucrose, 25 mM KCl, 5 mM MgCl2, 20 mM Tris-HCl pH 7.5) with Triton X-100 (Sigma-Aldrich, Cat#T8787) to a final concentration of 0.5%. The homogenates were then incubated for 15 minutes at 4°C followed by centrifugation at 3,200 xg for 5 minutes at 4°C, and the supernatants were discarded.

Samples were resuspended in 1x PBS containing 2% formaldehyde (Agar Scientifics, Cat#R1026) and incubated in a rocker for 10 min at room temperature. Formaldehyde was quenched with glycine to a final concentration of 0.125 M and incubated for 5 min at room temperature followed by 15 min at 4°C. Subsequently, the samples were washed with cold 1x PBS.

Neuronal nuclei purification

Neuronal nuclei were purified using fluorescence-activated nuclei sorting (FANS). Briefly, samples were stained with 7-AAD staining solution (Biolegend, Cat#420404; diluted 1:40, 5 μl/test) and Alexa Fluor®488-conjugated Anti-NeuN Antibody (clone A60, Millipore, Cat#MAB377X; diluted 1:2000), and then incubated overnight at 4°C. Stained samples were filtered through a 35 μm nylon mesh (Falcon, Cat#352235), and FANS was performed using MoFlo XDP High-Speed Cell Sorter (Beckman Coulter, Cat#ML99030) with Summit software (v5.2.0.7477). Neuronal nuclei were sorted intro DNA LoBind 1.5-ml tubes (Eppendorf, Cat#022431021), flash-frozen in dry-ice and stored at −80°C. For more details about sorting gates, see Figure S1.

Low input Promoter Capture Hi-C procedure

Neuronal nuclei samples from 9 mice per experimental group were used in Low input Promoter Capture Hi-C (liCHi-C).[115] Nuclei were thawed and centrifugated (1000xg at 4°C for 10 min), and the supernatant was discarded. Then pelleted nuclei were resuspended in ice-cold lysis buffer (10 mM Tris-HCl pH 8.0, 10 mM NaCl, 0.2% IGEPAL CA630 and 1× cOmplete EDTA-free protease inhibitor cocktail). Samples from 3 mice were pooled to obtain 10^6 nuclei per replicate, and liCHi-C was carried out with 3 replicates per experimental group.

Briefly, chromatin was digested overnight with HindIII enzyme (100 U/μL, New England Biolabs, Cat#R0104T). Then, the cohesive ends of the restriction fragments were filled-in with dGTP, dTTP, dCTT and biotin-14-dATP (Invitrogen, Cat#19524-016) using klenow polymerase (5 U/μL, New England Biolabs, Cat#M0210L). Blunt ends of the fragments were ligated with T4 DNA Ligase (1U/μl, Invitrogen, Cat#15224-025), and chromatin was decrosslinked overnight with proteinase K at 10 mg/ml (Roche, Cat#03115879001). DNA was isolated using phenol:chloroform:isoamyl alcohol 25:24:1 (Sigma-Aldrich, Cat#P3803) extraction, and quantified using Qubit 3.0 fluorometer (Invitrogen, Cat#Q33216).

DNA was sheared to an average size of 400 bp using M220 Focused-ultrasonicator (Covaris). Biotinylated ligated products were pulled down using Dynabeads MyOne streptavidin C1 paramagnetic beads (Thermo Fisher, Cat#65001). DNA was repaired and fragment ends were dATP-tailed and ligated to PE Illumina adapters (Table S9). The library was then amplified for 8–9 cycles by PCR, and purified by double-sided selection using SPRI beads (0.4–1 volumes, CleanNA, Cat#CNGS-0050). DNA concentration was determined using an Agilent 2200 TapeStation (Agilent, Cat#G2964AA) with D1000 ScreenTape Analysis (Agilent, Cat# 5067–5582).

Ligation products containing promoters were captured using the SureSelectXT Target Enrichment System for the Illumina Platform (Agilent Technologies), following manufacturer's instructions. The captured library was amplified for 4 cycles by PCR and purified using SPRI beads (0.9 volumes). Neuronal liCHi-C libraries were paired-end sequenced by BGI Genomics using DNBseq 100 + 100PE platform (MGI).

LiCHi-C processing

Paired-end reads were processed using HiCUP[52] (v0.8.3). First, the reference genome (*Mus musculus* GRCm38/mm10, Ensembl release 100) was indexed by Bowtie2[98] (v2.4.1) and computationally digested using the HiCUP Digester tool with HindIII restrictions sequences. Subsequently, reads were truncated using the HiCUP Truncater tool and aligned individually to the digested reference genome using the HiCUP Mapper tool. Experimental artifacts and duplicated reads were removed using the HiCUP Filter and Deduplicator tools. Paired reads that did not overlap with captured fragments in either case, were filtered out. Consequently, we retained only unique valid captured reads, allowing for the calculation of capture efficiency. Library statistics for all samples are presented in Table S1.

LiCHi-C interaction calling

Promoter interactions were called using CHiCAGO R package[53,99] (v1.18.0) with default parameters. CHiCAGO implements a statistical model with two components: biological noise (based on detected random interactions) and technical noise (based on experimental artifacts); along with normalization and multiple testing methods. Samples were analyzed individually, as well as merged samples, to increase sensitivity between experimental conditions. Unlocalised and unplaced scaffolds were filtered. Interactions are considered significant if they have a CHiCAGO score ≥ 5. Interaction statistics for all samples are presented in Table S1.

Histone and chromatin state enrichment

Chip-seq datasets for hippocampus tissue from a previous study[51] with four experimental conditions (YC, YE, OC, OE) were used for enrichment analyses of histone marks and chromatin states in the interacting regions. We used the 15 chromatin states established in that work: Promoter-Active (Pr-A), Promoter Weak (Pr-W), Promoter Bivalent (Pr-B), Promoter Flanking Region (Pr-F), Enhancer Strong TSS-distal (En-Sd), Enhancer Strong TSS-proximal (En-Sp), Enhancer Poised TSS-distal (En-Pd), Transcription Strong (Tr-S), Transcription Strong-2 (Tr-S2), Transcription Permissive (Tr-P), Transcription Initiation (Tr-I), Heterochromatin Polycomb-associated (Hc-P), Heterochromatin H3K9me3-associated (Hc-H), Heterochromatin Polycomb-associated weak (Hc-Pw) and No significant signal (Ns). Enrichments were carried out using CHiCAGO significant interactions in *cis*, and the peakEnrichment4Features function of the CHiCAGO R package. Ratios were calculated by comparing significant interaction overlaps and random sampling overlaps, and differential ratios (Δ Ratio) were calculated by subtracting control condition from the other condition. Finally, enrichments were visualized with the pheatmap package (v1.0.12).[100]

Differential analysis of interactions

Differential analysis between experimental conditions were computed using Chicdiff R package[55] (v0.6) with the default parameters. Chicdiff utilizes CHiCAGO data converted by makePeakMatrix CHiCAGO tool that spreads the ''Other End'' region generating an interaction peak matrix. The analysis was carried out on interactions with a CHiCAGO score cutoff greater than 5 on merged samples data for either of the compared conditions. We obtain Fold Change and p-value information of differential interactions between conditions. Interaction landscape with CHiCAGO and Chicdiff tracks was plotted with plotdiffBaits function.

Differential analysis of histone marks

Chip-seq datasets for hippocampus tissue from a previous study[51] with four experimental conditions (YC, YE, OC, OE) were used in the differential analysis of common histone marks (H3K27ac, H3K4me3, H3K4me1, H3K36me3, H3K27me3, H3K9me3). Normalization and differential analysis were performed using R/Bioconductor package DiffBind[101] (v3.0.15). Then, significant histone marks peaks (p-value < 0.05) were annotated to promoters and interacting regions displaying significantly enriched or depleted interactions, using the R/Bioconductor package GenomicRanges[102] (v1.54.1).

Gene ontologies enrichment analysis

We used the clusterProfiler[103] (v4.10.0) R package to determine the enrichment of Gene Ontology (GO) term for biological processes (BP) with gene promoters exhibiting significantly altered interactions. Specific parameters were: org.Mm.eg.db for the organism and Benjamini-Hochberg for the method for adjustment. Ontology terms with less than 15 genes or more than 2000 genes were filtered out. A q-value threshold of 0.05 was applied, and results with odds ratio greater than 6 were limited to 6. GO term enrichment was performed using all available BP-GO terms or focusing on Nervous system-associated BP-GO terms. The BP-GO terms most closely associated with the nervous system were selected and updated from Neural-Immune Gene Ontology (NIGO)[95] and Synaptic Gene Ontologies (SynGO)[96] subsets (Table S10). For captured fragments associated with multiple gene promoters, we prioritize protein-coding genes for GO analysis. All the genes in the capture design were considered the universe, and odds ratio was calculated comparing a given gene dataset to the universe. For clearer visualization, similar GO terms were grouped using an in-house pipeline based on the clustering algorithm from the rrvgo[104] (v1.14.1) R package.

RNA extraction and library preparation

Total RNA from fresh-frozen dorsal hippocampi was extracted from 6 mice per group (three biological replicates per condition) using RNeasy Mini Kit (Qiagen, Cat#74104) following manufacturer's protocol, and including DNase treatment (Qiagen, Cat#79254). RNA concentration was quantified using Qubit RNA HS Assay kit (Thermo Fisher Scientific, Cat#Q32852) and RNA integrity assessment was performed using Agilent 5300 Fragment Analyzer System (Agilent Technologies, Cat#M5311AA). Library preparation was conducted with NEBNext Ultra II RNA Library Prep Kit (New England Biolabs, Cat#E7770), including polyA selection, following manufacturer's instructions. Finally, the mRNA-seq libraries were sequenced, generating 150 bp paired-end reads on an Illumina NovaSeq 6000 Sequencing System (Illumina).

RNA-seq processing

The preprocessing and quality control of FASTQ files were conducted using fastp[105] (v0.20.1) with the options: -r -M 10 -l 20 -p -x –adapter_fasta. Salmon[106] (v1.5.0) was used for transcript-level quantification using the following options: –libType A –validateMappings –seqBias –gcBias. For the pseudo-alignment, a decoy-aware index gentrome was constructed from the mm10 genome and transcriptome. All the downstream analysis and processing were carried out within R: transcript-level RNA-seq quantification files from Salmon were imported into R and aggregated to the gene level through the R/Bioconductor package tximport[107] (v1.14.2). Ensembl IDs were annotated to gene symbols using the R/Bioconductor package biomaRt[108] (v2.42.0). mapping details are presented in Table S4.

Differential gene expression analysis

After aggregating transcript-level estimated counts to the gene level with tximport[107] (v1.14.2), low-expression genes were filtered out with the filterByExpr() function of the R/Bioconductor package edgeR[109] (v3.28.1). Subsequently, differentially expressed genes (DEGs) were identified from filtered gene-level estimated counts using the R/Bioconductor package DESeq2[110] (v1.26.0) with generalized linear models. Differential analyses were performed for three comparisons: Aging (old vs. young), EE in young mice (YEE vs. young) and EE in old mice (OEE vs old). DEGs were determined with an adjusted p-value significance level of 0.05, yet unadjusted p-value of 0.05 were used in some representations and integrations. Visualization of results as well as other analyses (e.g., PCA or GSEA analysis) were conducted using variance-stabilizing transformed (VST) values, obtained with the vst function of DESeq2. Genes with bivalent promoter were defined using Chip-seq data from a previous study[51] in each of the experimental conditions (YC, YE, OC, OE).

Principal component analysis

Principal component analysis (PCA) was conducted using the plot3d function of rgl package[111] (v1.2.1) with default parameters. PCA was performed with VST expression of the 2000 most variable genes and with the *scale* parameter.

Gene set enrichment analysis

Gene Set Enrichment Analysis (GSEA)[57] (v4.3.2) was performed using the VST expression data, to determine molecular pathways considering the fold change of all studied genes. M2 (curated gene sets) and M5 (ontology gene sets) collections, from the mouse MSigDB[97] v2023.1 (Molecular signatures database), were used in the enrichment analysis. Significant gene sets were selected with an FDR significance level of 0.05. LEIN markets dataset[70] was used for a specific enrichment analysis of mouse brain markers.

Data visualization

Result plots were generated using the ggplot2[112] (v3.4.2) R package, as well as the eulerr package[113] (v7.0.2) for Venn diagram. An in-house pipeline was employed to create virtual 4C plots of individual gene promoters. To visualize significant interactions (CHiCAGO score $\geq$ 5) and genomic regions with significantly altered interactions (Chicdiff), as well as to generate chord plots and circle plots, the WashU Epigenome Browser[114] (v54.0.3) was used.

QUANTIFICATION AND STATISTICAL ANALYSIS

Statistical analysis

Statistical analyses were performed using R software. Data are reported as mean values with standard deviation (SD). For comparisons between two groups, the Wilcoxon rank-sum test was used for unpaired samples, while paired samples were examined with the Wilcoxon signed-rank test. Probabilities were calculated using the hypergeometric distribution to study overlaps between groups. Associations between processes were examined using Pearson's correlation, and linear models were fitted using the *lm* function (Stats package). Level of significance is indicated with nsp-value > 0.05, *p-value < 0.05, **p-value < 0.01, ***p-value < 0.001. Additional statistical details are provided in each figure legend.